



DSM-based design proposal for CFS columns failing in local-distortional interactive modes

André Dias Martins¹, Dinar Camotim², Pedro Borges Dinis³, Ben Young⁴, Man-Tai Chen⁵

Abstract

This work proposes an efficient and rational approach, based on the Direct Strength Method (DSM), for the design of CFS columns failing in local-distortional (L-D) interactive modes. The development, calibration and validation of this design proposal, which is intended for codification in the near future, is based mostly on available experimental failure load data (*i.e.*, keeping in line with the DSM “tradition”), but benefits also from significant numerical failure load data involving columns with several cross-section shapes (plain, web-stiffened and web-flange-stiffened lipped channels, hat, zed and rack-sections). Three types of L-D interactive failures are covered, namely those due to “true L-D interaction”, “secondary-distortional bifurcation L-D interaction” and “secondary-local bifurcation L-D interaction” – naturally, the current DSM local and distortional strength curves are also linked to the current proposal. The merits (accuracy and safety) and reliability of the proposed DSM-based design approach are assessed – the latter following the procedure prescribed by the current North American Specification for the Design of Cold-Formed Steel Structural Members and are also compared with those exhibited by the existing methodologies to design CFS columns against L-D interactive failures.

1. Introduction

Cold-formed steel (CFS) members invariably display very slender thin-walled open cross-sections, a feature responsible for their high susceptibility to individual (local – L, distortional – D, global – G) or coupled (L-G, L-D, D-G, L-D-G) buckling phenomena. Nowadays, it is consensual amongst the technical/scientific community the need to have efficient design approaches to handle interactive failures, a goal that has long been achieved for L-G ones, both in cold-formed and hot-rolled steel members. Concerning interactive failures involving distortional buckling, *i.e.*, L-D, D-G or L-D-G ones, virtually exclusive of CFS members, due to the complex shapes often employed, the situation is completely different and the development of adequate design approaches requires in-depth knowledge about the response of members affected by the coupling phenomenon under scrutiny. Indeed, these interaction phenomena provide additional sources of ultimate strength erosion not adequately covered (or, sometimes, even mentioned) by any CFS design specification around the world. As far as CFS columns

¹ Postdoctoral Researcher, Instituto Superior Técnico, University of Lisbon, <andrerdmartins@tecnico.ulisboa.pt>

² Professor, Instituto Superior Técnico, University of Lisbon, <dcamotim@civil.ist.utl.pt>

³ Assistant Professor, Instituto Superior Técnico, University of Lisbon, <dinis@civil.ist.utl.pt>

⁴ Professor, The Hong Kong Polytechnic University, <ben.young@polyu.edu.hk>

⁵ Assistant Professor, Shanghai Jiao Tong University, <mantai.chen@sjtu.edu.cn>

undergoing L-D interaction is concerned, such knowledge already exists, mainly due to the authors' efforts. Thus, it may be argued that only the development and codification of a rational and efficient design approach are lacking – to bridge this gap is precisely the goal of this work.

The Direct Strength Method (DSM – *e.g.*, Camotim *et al.* 2016 or Schafer 2019) is nowadays a widely accepted approach/method to develop design methodologies for a variety of CFS member limit states. Currently, the codified DSM column design curves concern only L, D, G and L-G failures, *i.e.*, the column nominal strength (P_n) is given by $P_n = \min\{P_{nL}, P_{nD}, P_{nG}, P_{nL-G}\}$ ⁶. The aim of this work is to provide a DSM-based expression accounting for L-D failures, often occurring in short-to-intermediate columns, which means that P_n will become $P_n = \min\{P_{nL}, P_{nD}, P_{nG}, P_{nL-G}, P_{nL-D}\}$ – P_{nL-D} is the column nominal strength against L-D interactive failures. Since a considerable research activity has been devoted to study the behavior of L-D interaction in CFS columns, a brief state-of-art review is presented and discussed next, including experimental investigations, numerical simulations and DSM-based design proposals.

Although a significant number of column specimens failing in L-D modes have been reported in the literature, it is fair to mention that not all of the associated test campaigns were carried out with the specific purpose of investigating the L-D coupling phenomenon. Nonetheless, at least 161 specimens failing in L-D modes have been reported in the literature (as discussed in Section 3), practically all of them involving fixed-ended columns. The available experimental results evidencing the occurrence of L-D interaction in CFS columns are due to (i) Kwon & Hancock (1992), Young & Rasmussen (1998), Kwon *et al.* (2009), Loughlan *et al.* (2012) and Young *et al.* (2013), for lipped channel columns, (ii) Kwon *et al.* (2005), for lipped channel and hat-section columns, (iii) Dinis *et al.* (2014a), for rack-section columns, (iv) Kwon & Hancock (1992), Kwon *et al.* (2009), Yap & Hancock (2011), He *et al.* (2014) and Chen *et al.* (2020), for web-stiffened lipped channel columns, (v) Yang & Hancock (2004) and Chen *et al.* (2020), for web-flange-stiffened lipped channel columns, and (vi) Yap & Hancock (2008), for columns with complex-stiffened cross-sections⁷. These failure load data play a decisive role in the DSM-based design approach proposed in this paper.

Concerning the numerical investigations addressing this phenomenon, several have been reported in the recent past, comprising shell finite element analyses (SFEA) and, to a lesser extent, Generalized Beam Theory (GBT)-based investigations. Silvestre *et al.* (2009, 2012) reported ABAQUS SFEA parametric studies involving 204 simply supported and 183 fixed-ended lipped channel columns characterized by critical distortional-to-local buckling load ratios (P_{crD}/P_{crL}) varying between 0.90 and 1.10. The authors proposed a novel DSM-based approach (NL-D approach) to predict L-D interactive failures for the two distinct boundary conditions and concluded that this approach led to accurate results. The assessment of the so-called NLD and NDL approaches, proposed by Schafer (2002), was also performed⁸. A few years later, Dinis & Camotim (2015) extended the findings reported earlier by Silvestre *et al.* (2012), for fixed-ended columns, to cover columns with other cross-section shapes, namely hat-sections, zed-sections and rack-sections, again involving columns with $0.90 \leq P_{crD}/P_{crL} \leq 1.10$. The authors were mainly interested in assessing the performance of the NL-D approach in predicting the failure loads of columns with the aforementioned cross-section shapes and they found that this approach is capable of accounting for the failure load erosion stemming from the L-D interaction detrimental effects. In the same year, Martins *et al.* (2015) reported an ABAQUS SFEA study on the relevance of L-D interaction effects on lipped channel, hat-section, zed-section and rack-section fixed-ended columns with $0.42 \leq P_{crD}/P_{crL} \leq 2.40$

⁶ The values of P_{nL} and P_{nL-G} are obtained from the same set of expressions.

⁷ Despite the unusual cross-section shape considered, it was decided to include these failure load results in this study.

⁸ As will be shown, the DSM NDL approach is at the root of the proposal made in this manuscript.

and covering also a wide (critical) slenderness range. This investigation showed that L-D interaction does not occur only when P_{crD} and P_{crL} are close, *i.e.*, the so-called “true L-D interaction”, and made it possible to unveil other L-D interaction types stemming from the (i) moderate distortional or (ii) high local post-critical strength: “secondary local-bifurcation L-D interaction” and “secondary distortional-bifurcation L-D interaction”, respectively. Although, the former may be ignored, since it causes negligible ultimate strength erosion, the latter is very relevant and must be accounted for in the design stage. Then, it was shown that the above findings apply also to fixed-ended web-stiffened and web-flange-stiffened lipped channel columns (Martins *et al.* 2016, 2017a). It is also worth noting that, in 2017, Martins *et al.* (2017b) proposed a preliminary DSM-based design approach to handle L-D failures. However, the limited amount of reliable test results available precluded a full validation of that design approach. This is why a fairly extensive test campaign was very recently carried out by Chen *et al.* (2020), at The University of Hong Kong – it enabled the proposal of the more rational design approach addressed in this work. Lastly, Martins *et al.* (2018a) reported an in-depth numerical investigation, based on GBT geometrically non-linear analyses, aimed at unveiling the mechanics underlying the behavior of simply supported and fixed-ended lipped channel columns undergoing “true” and “secondary local or distortional-bifurcation” L-D interaction. As will be shown, the knowledge acquired from these extensive numerical analyses was also very important for the developed of the proposed DSM-based design approach.

The paper outline is as follows. Section 2 addresses the relevance of the L-D interaction effects on the basis of numerical (shell finite element) analyses, while Section 3 presents the available experimental failure loads of columns experiencing L-D interaction. Then, Section 4 presents and discusses the DSM-based design approaches to handle column L-D interactive failures. After some initial considerations, included in Section 4.1, design proposals for “true L-D interaction” (Section 4.2), “secondary distortional-bifurcation L-D interaction” (Section 4.3) and “secondary local-bifurcation L-D interaction” (Section 4.4) are presented and amply discussed – the structural reliability assessment of each proposal is also provided, following the procedure prescribed by the North American Specification for the Design of Cold-Formed Steel Structural Members (AISI 2020). Lastly, Section 5 provides a few concluding remarks and highlights the most relevant findings reported in this work.

2. Relevance of Secondary-Bifurcation L-D Interaction

From the knowledge acquired in past investigations, it is now well known that “secondary distortional-bifurcation (SDB) L-D interaction” clearly erodes the CFS column failure loads, which makes the determination of a border/boundary between columns exhibiting pure local and SDB L-D interactive failures a crucial task in the development of an efficient design approach. Naturally, this task can only be performed on the basis of numerical failure load data. In 2015, Martins *et al.* (2015) proposed such a border in the context of lipped channel (C), hat-section (H), zed-section (Z) and rack-section (R) columns with R_{DL} buckling ratios up to 2.39. However, the current knowledge on the subject shows that it is important to extend that investigation until the SDB L-D interaction effects cease to occur (*i.e.*, until local failures appear for quite high local slenderness values), which happens well beyond $R_{DL}=2.39$. Therefore, in order to extend/complete the above study, C, H, Z, R and also WSLC (web-stiffened lipped channel) columns with 6 additional R_{DL} values were analyzed here, namely R_{DL} equal to 3.0, 4.0, 5.0, 6.0, 8.0 and 10.0 – the column geometries and relevant buckling load ratios are given in Tables A.1 to A.6, included in Appendix A. The post-buckling results and failure loads were obtained by means of ABAQUS SFE models (Simulia 2008) similar to those used previously by Martins *et al.* 2015 and considering (i) also critical-mode local initial geometrical imperfections and (ii) the aforementioned geometries with local slenderness values going up to $\lambda_L=4.0$. In order to identify the range of $R_{DL}-\lambda_L$ combinations leading to visible SDB L-D interaction, the columns with $R_{DL}\geq 3.0$ were analyzed for increasing

yield stresses (corresponding to prescribed λ_L values). As done by Martins *et al.* (2015), relatively small intervals, containing “ λ_L lower limits”, were determined to separate columns experiencing or not SDB L-D interaction. Since these bounded intervals were found to be quite small, it was decided to plot only their “mid points” (averages between their upper and lower bounds). For instance, in the case of the $R_{DL}=3.0$ C column the failure mode is local for $\lambda_L=2.50$ (lower bound), while relevant distortional deformations are observed for $\lambda_L=2.75$ (upper bound), which means that failure is governed by SDB L-D interaction. Therefore, the limit considered for this buckling load ratio is the interval mid-point, *i.e.*, $\lambda_L=2.625$. The λ_L - R_{DL} combinations summarized in Fig. 1(a) are the output of this study. For simplicity and clarity, it was decided to propose only one (conservative) border for all of the cross-section shapes considered, which is also displayed in Fig. 1(a) and is defined by $\lambda_L=0.40R_{DL}+0.60$ – *i.e.*, columns with given R_{DL} and λ_L values are expected to fail in local or SDB L-D interactive modes depending on whether $\lambda_L < 0.40R_{DL}+0.60$ or $\lambda_L > 0.40R_{DL}+0.60$, respectively.

Similarly, it is also possible to obtain a border between pure distortional and “secondary local-bifurcation (SLB)” L-D interactive failures. This has been done by Martins *et al.* (2015) for C, H, Z and R columns and is not extended here to cover also WSLC columns because local buckling is triggered by the flanges, where the emergence of local deformations is very difficult to track, unlike in the C, H, Z and R columns (web-triggered local buckling). Therefore, the sought border was defined solely on the basis of “plain web” cross-sections, and it was found to be (conservatively) defined by $\lambda_D=2.44-1.60R_{DL}$ – see Fig. 1(b). The two above borders are essential to develop the DSM-based design approach (see Sections 4.3 and 4.4).

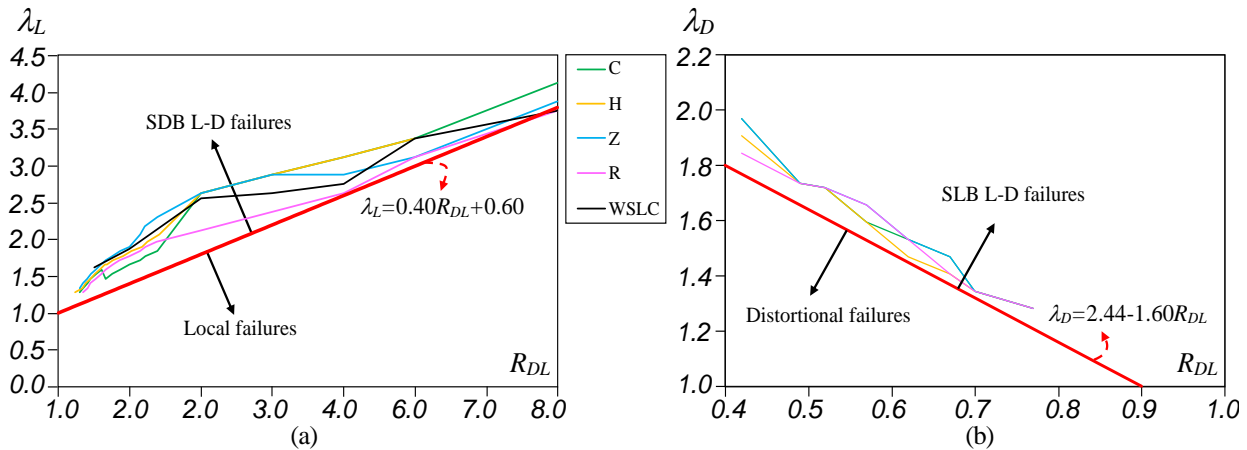


Figure 1: λ_L - R_{DL} or λ_D - R_{DL} combinations associated with the transition between (a) pure local and SDB L-D interactive failures (C, H, Z, R and WSLC columns) or (b) pure distortional and SLB L-D interactive failures (C, H, Z and R columns)

3. Available Experimental Failure Loads of CFS Columns Experiencing L-D interaction

Several test campaigns dealing with L-D interaction in CFS fixed-ended columns are currently available in the literature. However, it should also be mentioned that part of the L-D failures observed in these experimental investigations were obtained “by accident” – *e.g.*, when only a small fraction of the specimens belonging to a test campaign were observed to fail in L-D interactive modes. Nonetheless, a significant number of specimens providing clear experimental evidence of this coupling phenomenon, and of the ensuing failure load erosion, are currently available – a total of 161 specimens. Despite the considerable number of tests available, it should be noted that it is smaller than the number of tests considered to develop and calibrate the currently codified DSM local (P_{nL}) and distortional (P_{nD}) column strength curves (249 tests, according to Schafer 2008). As mentioned earlier, these experimental results evidencing the occurrence of L-D interaction in CFS fixed-ended columns are due to (i) Kwon &

Hancock (1992), Young & Rasmussen (1998), Kwon *et al.* (2009), Loughlan *et al.* (2012) and Young *et al.* (2013), for C columns, (ii) Kwon *et al.* (2005), for C and H columns, (iii) Dinis *et al.* (2014a), for R columns⁹, (iv) Kwon & Hancock (1992), Kwon *et al.* (2009), Yap & Hancock (2011), He *et al.* (2014) and Chen *et al.* (2020), for WSLC columns, (v) Yang & Hancock (2004) and Chen *et al.* (2020), for WFSLC columns, and (vi) Yap & Hancock (2008), for columns with complex-stiffened cross-sections (CSCS). Although Chen *et al.* (2019) originally claimed that six zed-section specimens (out of a total of 12) had failed in L-D interactive modes, a subsequent careful examination by the authors showed that, most likely, these specimens failed in pure local modes – this is because (i) the length-to-web width ratios are around 3.0 (*i.e.*, the specimens correspond to stub columns), (ii) the few photographs taken during the tests are compatible with typical local failures (even if “distortional-like deformations” appear at collapse, most likely due to the yielding of the web-flange corner regions, not distortional buckling) and (iii) the current DSM local design curve estimates accurately the specimen failure loads. Therefore, it was decided to not include these test results in the data base used in this work. Regarding the test results reported by Yap & Hancock (2006, 2008), it is worth mentioning that:

- (i) The tests involved columns with a complex cross-section (multiple stiffeners) that are susceptible to buckle in two distortional modes (besides the susceptibility to local and global buckling): they differ in the half-wave length size, one smaller (“short half-wavelength distortional buckling mode”) and the other larger (“long half-wavelength distortional buckling mode”).
- (ii) 15 tests were conducted for columns sharing the same cross-section dimensions and with 5 lengths ($L=110, 600, 1200, 1600$ and $2000\text{mm} - 3$ “repeated” tests per length). However, the $L=110\text{mm}$ columns failed in local modes and specimen SCR600_3 ($L=600\text{mm}$) was not tested, since it was used to extract the tensile coupons – *i.e.*, 11 specimens failed in different types of L-D interactive modes.
- (iii) The L-D interactive failure modes have distinct characteristics, as they combine (iii₁) local and short half-wave length distortional deformations ($L=600\text{mm}$), (iii₂) local and long half-wave length distortional deformations ($L=2000\text{mm}$) and (iii₃) local and short + long half-wave length distortional deformations ($L=1200$ and 1600mm) – the last failure modes are denoted as L-D² interactive.
- (iv) It should be clear for the reader, that most of the relevant information mentioned in the above three items was only provided in the technical report due to Yap & Hancock (2006) – surprisingly, it was not included in the ensuing journal paper (Yap & Hancock 2008). Moreover, the three buckling modes (1 local and 2 distortional) are associated with distinct buckling loads – the buckling load ratio R_{DL} varies between, 0.88 and 1.03, *i.e.*, the columns failed in True L-D interactive modes.

Table 1 summarizes the available test results for CFS fixed-ended columns experiencing L-D interaction. The measured geometrical and material properties (conventional yield stress and Young’s modulus¹⁰) were used to calculate the column squash (P_y) and critical local (P_{crL}), distortional (P_{crD}) and global (P_{crG}) buckling loads, by means of the GBTUL code (Bebiano *et al.* 2018). For organizational and clarification purposes, the test results were divided in seven sets, according to the specimen (i) cross-section shape (PCS, WSLC, WFSLC and CSCS, where PCS groups C, H, R cross-sections) and (ii) L-D interaction type (SLI, TI or SDI) – the numbers of specimens tested are given next to the reference in Table 1. The L-D interaction type was determined as follows (see also Section 2): (i) TI if $0.8 \leq P_{crD}/P_{crL} \leq 1.3$ (regardless of the yield stress value), (ii) SLI if $P_{crD}/P_{crL} < 0.8$ and (iii) SDI if $P_{crD}/P_{crL} > 1.3$.

⁹ Dinis *et al.* (2014b) reported the results of another test campaign, involving the WSLC columns. However, these results were not considered in this study, since no clear L-D failures were observed. In fact, this test campaign was originally planned to investigate D-G interaction – due to deficiencies in manufacturing the specimens, this goal was not achieved.

¹⁰ Either reported in the corresponding reference/work or assumed to be $E=210\text{GPa}$.

Table 1: Available test results concerning CFS columns experiencing L-D interaction

	SLI	TI	SDI
PCS (C, H, R)	Kwon & Hancock (1992): 1	Kwon & Hancock (1992): 4 Kwon <i>et al.</i> (2005): 3 Kwon <i>et al.</i> (2009): 1 Matsubara <i>et al.</i> (2019): 3	Young <i>et al.</i> (2013): 16 Loughlan <i>et al.</i> (2012): 20 Young & Rasmussen (1998): 3 Kwon <i>et al.</i> (2009): 5 Dinis <i>et al.</i> (2014a): 10
WSLC	Yap & Hancock (2011): 5	Kwon & Hancock (1992): 3 Kwon <i>et al.</i> (2009): 6 He <i>et al.</i> (2014): 15 Yap & Hancock (2011): 6 Chen <i>et al.</i> (2020): 11	Kwon <i>et al.</i> (2009): 3 He <i>et al.</i> (2014): 3 Chen <i>et al.</i> (2020): 4
WFSLC		Yang & Hancock (2004): 8 Chen <i>et al.</i> (2020): 14	Yang & Hancock (2004): 4 Chen <i>et al.</i> (2020): 2
CSCS		Yap & Hancock (2008): 11	
Total	6	85	70

4. DSM-Based Design Approach for Column L-D Interactive Failures

4.1 Background

4.1.1 Existing DSM-based design approaches

Several DSM-based design approaches intended to handle CFS column L-D interactive failures have been proposed in the recent past. Two of them are due to Schafer (2002): the NLD and NDL approaches, both based on the currently codified local (P_{nL})¹¹ and distortional (P_{nD}) DSM design curves. These “Winter-type” expressions are obtained by replacing P_y with either (i) P_{nD} in the P_{nL} equations (NLD approach – P_{nLD}) or (ii) P_{nL} in the P_{nD} equations (NDL approach – P_{nDL}), and read

$$P_{nDL} = \begin{cases} P_{nL} & , \quad \lambda_{DL} \leq 0.561 \\ P_{nL} \lambda_{DL}^{-1.2} (1 - 0.25 \lambda_{DL}^{-1.2}), & \lambda_{DL} > 0.561 \end{cases} \quad (1)$$

$$P_{nLD} = \begin{cases} P_{nD} & , \quad \lambda_{LD} \leq 0.776 \\ P_{nD} \lambda_{LD}^{-0.8} (1 - 0.15 \lambda_{LD}^{-0.8}), & \lambda_{LD} > 0.776 \end{cases} \quad (2)$$

where $\lambda_{DL} = (P_{nL}/P_{crD})^{0.5}$ and $\lambda_{LD} = (P_{nD}/P_{crL})^{0.5}$ are the distortional (local) slenderness based on the local (distortional) strength. The currently codified local and distortional design curves, appearing in Eqs. (1)-(2) and essential for the following developments, are given respectively by

$$P_{nL} = \begin{cases} P_y & , \quad \lambda_L \leq 0.776 \\ P_y \lambda_L^{-0.8} (1 - 0.15 \lambda_L^{-0.8}), & \lambda_L > 0.776 \end{cases} \quad (3)$$

$$P_{nD} = \begin{cases} P_y & , \quad \lambda_D \leq 0.561 \\ P_y \lambda_D^{-1.2} (1 - 0.25 \lambda_D^{-1.2}), & \lambda_D > 0.561 \end{cases} \quad (4)$$

where $\lambda_D = (P_y/P_{crD})^{0.5}$ and $\lambda_L = (P_y/P_{crL})^{0.5}$ are the distortional and local slenderness, respectively.

As noted earlier, the “generalized modified NDL approach” (MNDL) was first proposed by Silvestre *et al.* (2012), for C columns, and later extended to (i) H, Z and R columns by Dinis and Camotim (2015) and

¹¹The currently codified P_{nL} curve is intended to handle both pure local and L-G interactive failures – in fact, it may be said that it is a P_{nLG} curve. In this work the “pure” P_{nL} curve is considered, *i.e.*, that obtained from the currently codified one by replacing P_{nG} with P_y – see Eq. (3).

(ii) to WSLC and WFSLC columns by Martins *et al.* (2016, 2017a) – SFEA numerical failure loads always used for validation/calibration. This design approach requires defining a modified local strength P_{nL}^* , dependent on the column critical half-wave length ratio L_{crD}/L_{crL} (obtained from simply supported column “signature curves”), and estimates the column failure loads by replacing P_{nL} with P_{nL}^* in the NDL approach (Eq. 1)¹². This modified local strength leads to P_{nD} and P_{nDL} estimates for $L_{crD}/L_{crL} \leq a$ and $L_{crD}/L_{crL} \geq b$, respectively. The integers “ a ” and “ b ” vary with the cross-section shape: (i) $a=4 + b=8$ (C, H, Z, R), (ii) $a=8 + b=12$ (WSLC) and (iii) $a=14 + b=40$ (WFSLC). The P_{MnDL} approach is then given by

$$P_{MnDL} = \begin{cases} P_{nL}^* & , \quad \lambda_{DL}^* \leq 0.561 \\ P_{nL}^* \lambda_{DL}^{*-1.2} (1 - 0.25\lambda_{DL}^{*-1.2}) & , \quad \lambda_{DL}^* > 0.561 \end{cases} \quad (5)$$

with

$$P_{nL}^* = \begin{cases} P_y & , \quad \frac{L_{crD}}{L_{crL}} \leq a \\ P_y + \left(\frac{a}{b-a} - \frac{1}{b-a} \frac{L_{crD}}{L_{crL}} \right) (P_y - P_{nL}) & , \quad a \leq \frac{L_{crD}}{L_{crL}} \leq b \\ P_{nL} & , \quad \frac{L_{crD}}{L_{crL}} \geq b \end{cases} \quad (6)$$

where $\lambda_{DL}^* = (P_{nL}^*/P_{crD})^{0.5}$ denotes the distortional slenderness based on the modified local strength P_{nL}^* .

To compare the failure load estimates provided by the five design curves (NL, ND, NDL, NLD, MNDL), Fig. 2(a) plots the P_{nL}/P_y , P_{nD}/P_y , P_{nDL}/P_y , P_{nLD}/P_y and P_{nMnDL}/P_y values against the local or distortional slenderness (assuming $\lambda_D = \lambda_L$). This figure shows (i) that the local post-critical strength is much higher than the distortional one, (ii) the failure load erosion inherent to L-D interaction and (iii) that the NDL and NLD approaches are very similar, even if only for close $P_{crD} \approx P_{crL}$ ($P_{crD} = P_{crL}$ in the case illustrated).

Recently, Martins *et al.* (2017b) proposed a novel DSM-based approach, termed NSDB and intended to handle columns prone to SDI L-D interaction. It combines (i) the NL design curve, for $\lambda_L \leq 0.85P_{crD}/P_{crL}$, (ii) a “Winter-type” curve, for $\lambda_L \geq 0.85P_{crD}/P_{crL} + \Delta\lambda_L$, and (iii) a linear transition between these two curves (occurring in the $\Delta\lambda_L = \lambda_{L2} - \lambda_{L1}$ range) – this approach, illustrated in Fig. 2(b), is defined by

$$P_{nSDB} = \begin{cases} P_{nL} & , \quad \lambda_L \leq \lambda_{L1} \\ P_1 + \frac{P_2 - P_1}{\lambda_{L2} - \lambda_{L1}} (\lambda_L - \lambda_{L1}) & , \quad \lambda_{L1} < \lambda_L < \lambda_{L2} \\ P_y \lambda_L^{-a} (1 - b\lambda_L^{-a}) & , \quad \lambda_L \geq \lambda_{L2} \end{cases} \quad (7)$$

where the various parameters (also indicated in Fig. 2(b)) are given by

$$P_1 = P_{y1} \lambda_{L1}^{-0.8} (1 - 0.15\lambda_{L1}^{-0.8}) \quad P_2 = P_{y2} \lambda_{L2}^{-a} (1 - b\lambda_{L2}^{-a}) \quad (8a)$$

$$\lambda_{L1} = m \frac{P_{crD}}{P_{crL}} \quad \lambda_{L2} = \lambda_{L1} + \Delta\lambda_L \quad P_{y1} = \lambda_{L1}^2 P_{crL} \quad P_{y2} = \lambda_{L2}^2 P_{crL} \quad (8b)$$

with $\Delta\lambda_L = 0.25$ and the pair $a=1.20$, $b=0.15$ obtained from an optimization procedure.

¹²The original design approach adopted the P_{nD} design curve for stocky columns ($\lambda_D < 1.5$). However, following the imperfection sensitivity study reported by Martins *et al.* (2017b), this design curve ceased to be adopted.

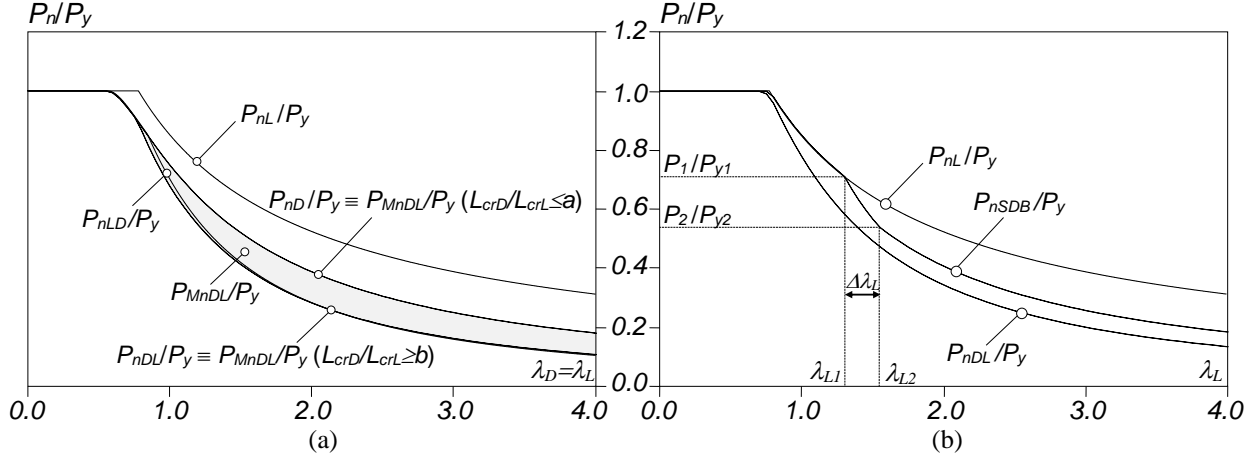


Figure 2: Available DSM-based (a) NL, ND, NLD, NDL, MNDL (assuming $\lambda_D = \lambda_L$) and (b) NSDB design approaches

4.1.2 Structural Reliability Assessment

The merit of the DSM-based design approaches addressed in the next sub-sections is assessed through the evaluation of the LRFD (Load and Resistance Factor Design) resistance factor ϕ , prescribed by the North American Specification (NAS) for Cold-Formed Steel Structures (AISI 2020). According to its Section K2.1.1, based on the work of Hsiao (1988) and Hsiao *et al.* (1988), ϕ is given by

$$\phi = C_\phi M_m F_m P_m e^{-\beta_o \sqrt{V_M^2 + V_F^2 + C_p V_p^2 + V_Q^2}} \quad (9)$$

where (i) $C_\phi = 1.52$ (calibration coefficient for LRFD), (ii) $M_m = 1.10$, $F_m = 1.00$ are the material and fabrication factor mean values (taken from Table K2.1.1-1 of that specification, corresponding to compressed members), (iii) β_o is the target reliability value ($\beta_o = 2.5$ for structural members in LRFD), (iv) $V_F = 0.05$ (again taken from Table K2.1.1-1 of that same specification) and $V_Q = 0.21$ are the fabrication factor and load effect coefficients of variation, respectively, (v) C_p is a correction factor dependent on the number of tests, and (vi) P_m and V_p are the mean and coefficient of variation of the “exact”-to-predicted failure load ratios. Regarding the mean and coefficient of variation of the material factor (M_m and V_M), two sets are considered in this study: (i) the values provided in Table K2.1.1-1 of AISI (2020) ($M_m = 1.10$ and $V_M = 0.10$), more suitable for the traditional lower steel grades and (ii) $M_m = 1.192$ and $V_M = 0.031$, taken from Pham & Hancock (2012) and more suitable for high-strength steels – the corresponding resistance factors are ϕ_1 and ϕ_2 ($> \phi_1$), respectively. The minimum value recommended for compressed members is $\phi_c = 0.85$, regardless of the failure mode nature (local, distortional, global or interactive) – thus, all the proposed DSM-based design approaches discussed in the next sub-sections should provide resistance factors $\phi \geq 0.85$.

4.2 True L-D Interaction

To the authors’ best knowledge, the three most rational DSM-based design approaches to handle True L-D interaction are the NDL, NLD and MNDL approaches. However, since the first two approaches yield essentially the same failure load estimates for columns with close P_{crL} and P_{crD} values (see Fig. 2(a)), only the NDL¹³ and MNDL approaches are addressed here. As noted earlier, the proposed DSM-based design approaches are mainly based on experimental failure load data, thus preserving the DSM essence – however, extensive numerical failure load data obtained by the authors are also considered.

¹³ The NLD is discarded since the NDL approach contains useful features that influence the design proposal addressed in Section 4.3.

Figs. 3(a)-(b) show plots P_{Exp}/P_{nDL} vs. λ_D and P_{Exp}/P_{MnDL} vs. λ_D for all the available experimental failure loads of columns susceptible to True L-D interaction (74 specimens with C, H, WSLC and WFSLC cross-sections – see Table 1). As for Figs. 4(a)-(f) and 5(a)-(f) show, respectively, plots P_U/P_{nDL} vs. λ_D and P_U/P_{MnDL} vs. λ_D for the numerical failure loads obtained by the authors (Martins *et al.* 2015, 2016, 2017a) – the values concerning the C, H, Z, R, WSLC, WFSLC columns are plotted separately. Lastly, Tables 2 and 3 show the n (number of failure loads or specimens), P_m , V_p and ϕ (ϕ_1 and ϕ_2) values concerning the NDL and MNDL estimates of the experimental and numerical failure loads, respectively. The careful examination of these results makes it possible to conclude that:

- (i) The NDL approach clearly outperforms its MNDL counterpart in predicting the experimental failure loads of columns undergoing True L-D interaction, as attested by the experimental-to-predicted load ratio (i_1) mean value and coefficient of variation (CoV) (1.06 + 13% vs. 0.86 + 12%) and (i_2) resistance factor ($\phi_1=0.90$ vs. $\phi_1=0.74$) – see Figs. 3(a)-(b) and Table 2. Naturally, if $M_m=1.192$ and $V_M=0.031$ are considered, the resistance factors increase considerably ($\phi_2=1.01$ vs. $\phi_2=0.83$). Moreover, mainly due to the recent test campaign carried out by Chen *et al.* (2020), there is a very clear improvement of the NDL approach performance, with respect to that observed against the failure load data available in 2017, which led to the preliminary DSM-based design approach proposed by Martins *et al.* (2017b). Indeed, the mean (CoV) P_{Exp}/P_{nDL} value is now higher (lower) for a significantly larger number of tests results (85 vs. 47), thus leading to a higher resistance factor.

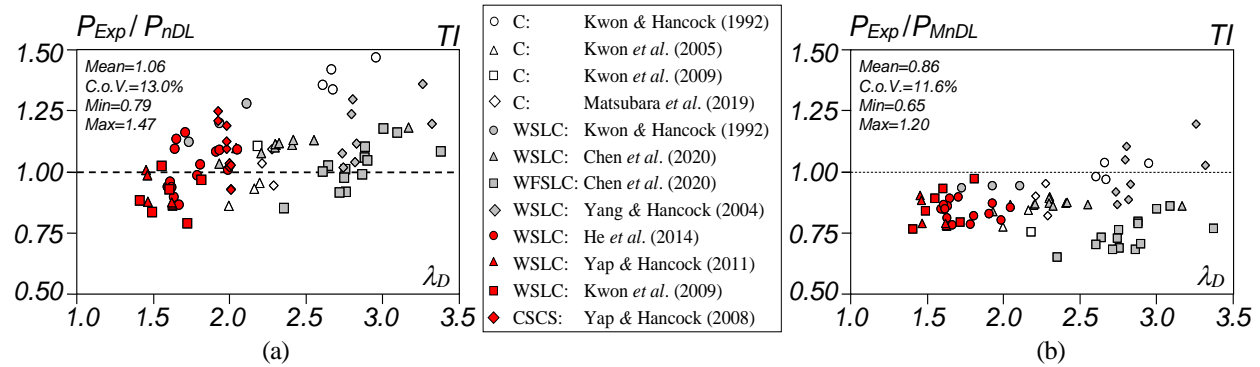


Figure 3: Plots (a) P_{Exp}/P_{nDL} vs. λ_D and (b) P_{Exp}/P_{MnDL} vs. λ_D concerning all the available experimental failure loads of columns undergoing True L-D interaction

Table 2: LRFD resistance factors ϕ according to AISI (2020) concerning all the available experimental failure loads of columns undergoing True L-D interaction: NDL and MNDL approaches

Cross-section	Reference	n	NDL				MNDL			
			P_m	V_p	ϕ_1	ϕ_2	P_m	V_p	ϕ_1	ϕ_2
C	Kwon & Hancock (1992)	4	1.40	0.04	1.24	1.41	1.00	0.04	0.90	1.03
H	Kwon <i>et al.</i> (2005)	3	0.92	0.05	0.78	0.88	0.83	0.06	0.70	0.79
C	Kwon <i>et al.</i> (2009)	1	1.11	0.00	1.02	1.16	0.75	0.00	0.69	0.79
C	Matsubara <i>et al.</i> (2019)	3	1.02	0.07	0.82	0.92	0.89	0.08	0.71	0.80
WSLC	Kwon & Hancock (1992)	3	1.20	0.07	0.99	1.11	0.94	0.00	0.86	0.98
WSLC	Yap & Hancock (2011)	6	0.91	0.07	0.80	0.91	0.82	0.07	0.72	0.82
WSLC	Kwon <i>et al.</i> (2009)	6	0.91	0.10	0.77	0.87	0.86	0.09	0.73	0.83
WSLC	He <i>et al.</i> (2014)	14	1.02	0.09	0.89	1.01	0.84	0.04	0.76	0.87
WFSLC	Yang & Hancock (2004)	8	1.17	0.11	0.99	1.12	1.00	0.12	0.83	0.94
WSLC	Chen <i>et al.</i> (2020)	11	1.11	0.03	1.02	1.16	0.87	0.02	0.80	0.91
WFSLC	Chen <i>et al.</i> (2020)	14	1.02	0.09	0.90	1.02	0.74	0.09	0.65	0.74
CSCS	Yap & Hancock (2008)	11	1.08	0.10	0.93	1.05	-	-	-	-
Total		85	1.06	0.13	0.90	1.01	0.86	0.12	0.74	0.83

As also observed by Martins *et al.* (2017b), the failure loads reported by Kwon *et al.* (2005, 2009) are substantially overestimated, while the four C column failure loads reported by Kwon & Hancock (1992) are significantly underestimated. It is also worth noting that the failure loads reported by Dinis *et al.* (2014b), not considered in this work (recall footnote 9), are adequately predicted by the NDL approach: P_U/P_{nDL} mean value and CoV and ϕ_l equal to 0.95, 2.5% and 0.87, respectively.

- (ii) Concerning the numerical failure load data, Fig. 4(a)-(f) and 5(a)-(f) show that the NDL approach outperforms its MNDL counterpart for WSLC and WFSLC columns, since the latter overestimates a significant number of failure loads. For the remaining four cross-sections, the NDL approach yields conservative failure loads, as attested by the P_U/P_{nDL} statistical indicators provided in the figures (note that the minimum value is very close to 1.0 for all the column sets), while the P_U/P_{MnDL} mean values are all closer to 1.0 with a relatively low CoVs (below 10%), although there is a significant number of P_U/P_{MnDL} values below 1.0 (especially for C, WSLC and WFSLC columns – see Figs. 5(a)+(e)+(f)). The resistance factors given in Table 3 corroborate the above assertions – *e.g.*, the resistance factors (ϕ_l) associated with the MNDL approach and regarding the WSLC and WFSLC columns are the lowest ones in that table. Nonetheless, considering all the 1421 column failure loads, the resistance factor is equal to 1.08 and 0.93 for the NDL and MNDL approaches, respectively – both fulfill the target reliability by a significant margin.
- (iii) It is worth noting that, due to the influence of the initial geometrical imperfection shape, there is a higher variability associated with the experimental failure loads. This is particularly noticeable in columns buckling in single distortional half-wave modes, because of a very clear asymmetry, first unveiled by Prola & Camotim (2002) and later confirmed by Martins *et al.* (2016, 2017a): the post-critical strengths of columns exhibiting outward and inward flange-lip motions are always different (depending on the cross-section shape, one or the other may be the highest). This asymmetry was observed experimentally by Yap & Hancock (2011) and Yang & Hancock (2011), in the context of WSLC and WFSLC columns sharing the same cross-section dimensions. It increases the CoV

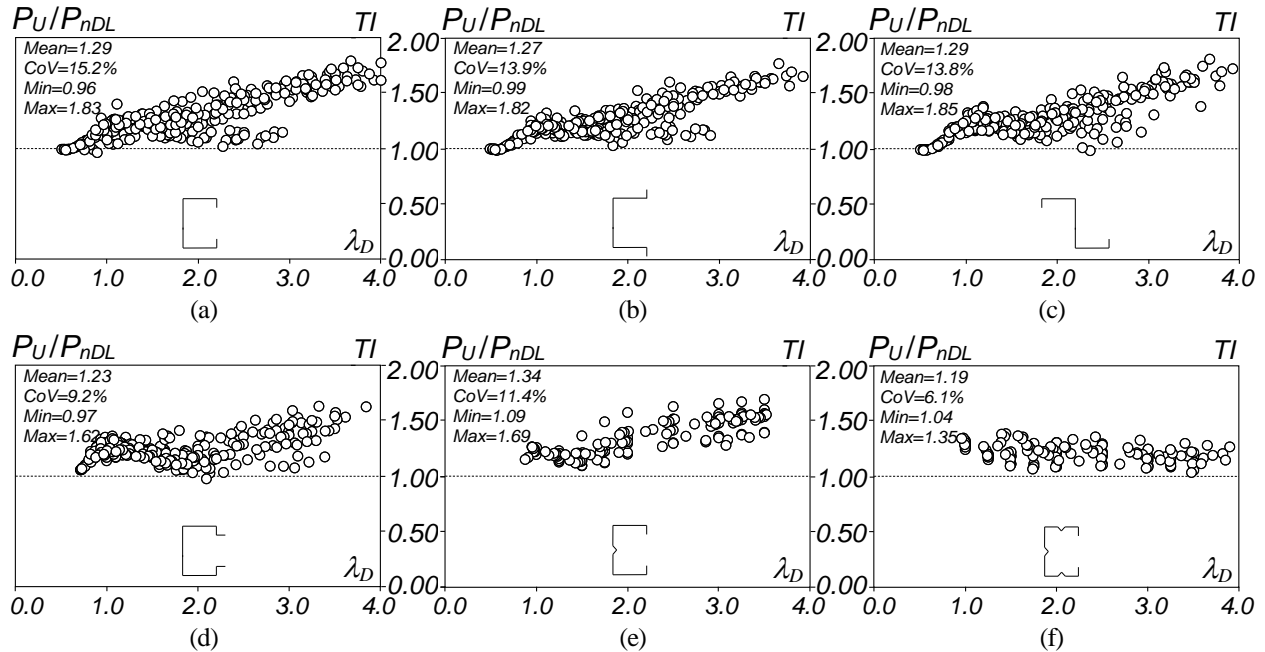


Figure 4: Plots P_U/P_{nDL} vs. λ_D concerning the numerical failure loads of columns undergoing True L-D interaction: (a) C, (b) H, (c) Z, (d) R, (e) WSLC and (f) WFSLC columns

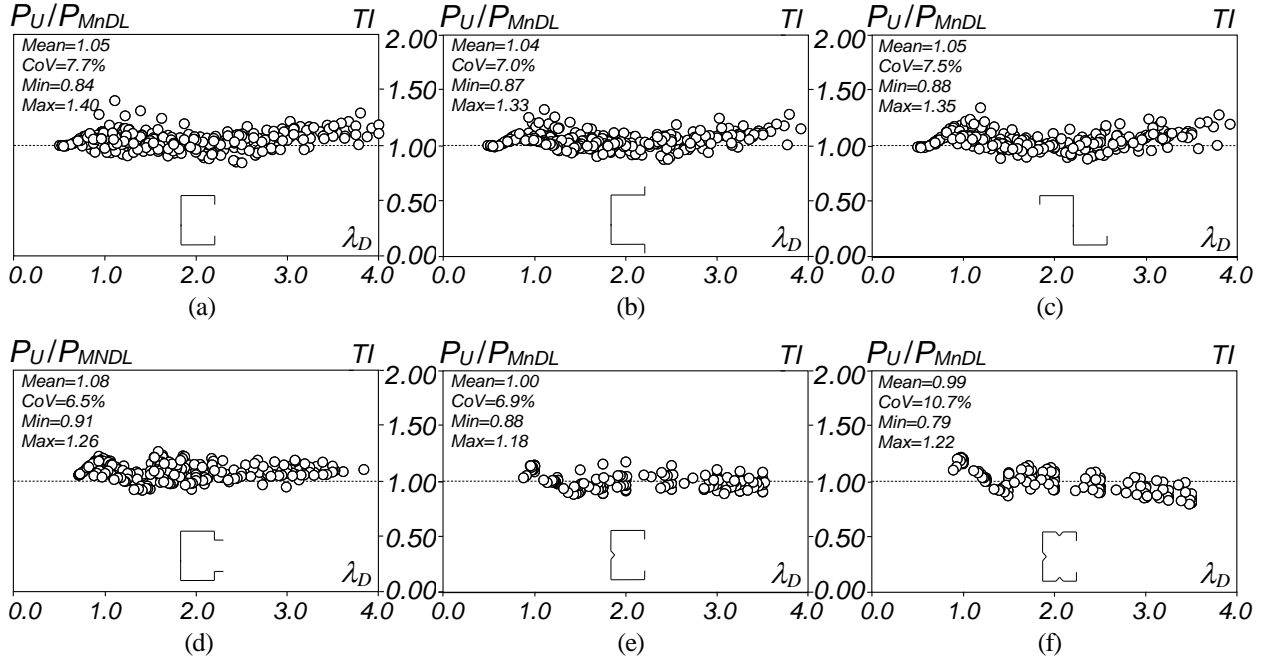


Figure 5: Plots P_U/P_{MnDL} vs. λ_D concerning the numerical failure loads of columns undergoing True L-D interaction: (a) C, (b) H, (c) Z, (d) R, (e) WSLC, (f) WFSLC columns

Table 3: LRFD resistance factors ϕ according to AISI (2020) concerning the numerical failure loads of columns undergoing True L-D interaction: NDL and MNDL approaches

Cross-section	Source	n	NDL			MNDL		
			P_m	V_p	ϕ_l	P_m	V_p	ϕ_l
C	Martins <i>et al.</i> (2015) + Dinis & Camotim (2015)	285	1.29	0.15	1.06	1.05	0.08	0.93
H	Martins <i>et al.</i> (2015) + Dinis & Camotim (2015)	269	1.27	0.14	1.07	1.04	0.07	0.94
Z	Martins <i>et al.</i> (2015) + Dinis & Camotim (2015)	279	1.29	0.14	1.08	1.05	0.07	0.94
R	Martins <i>et al.</i> (2015) + Dinis & Camotim (2015)	304	1.23	0.09	1.09	1.08	0.07	0.97
WSLC	Martins <i>et al.</i> (2016)	144	1.34	0.11	1.16	1.00	0.07	0.90
WFSLC	Martins <i>et al.</i> (2017a)	140	1.19	0.06	1.08	0.99	0.11	0.86
Total		1421	1.27	0.13	1.08	1.04	0.08	0.93

of the experimental-to-predicted failure load ratios, leading to lower resistance factors, while it does not influence the numerical failure loads, always concerning the most detrimental based initial geometrical imperfection shape. Naturally, these comments also apply to the failure load predictions and reliability assessments discussed in Sections 4.3 and 4.4.

- (iv) Taking into account the content of the previous items, it is clear that the NDL approach is able to handle adequately columns undergoing True L-D interaction, which exhibit severe failure load erosion – thus, its codification is recommended. It is also worth noting that the resistance factor associated with this design approach ($\phi_l=0.90$) coincides with that obtained for the currently codified ND curve and is significantly higher than that obtained for the currently codified NL curve ($\phi=0.79$) – see Schafer (2008).

4.3 Secondary-Distortional Bifurcation L-D Interaction

It has been unequivocally shown, both experimentally and numerically, that SDB L-D interaction must be taken into account to avoid a high likelihood of reaching unsafe designs. This is because the well

known very pronounced local post-critical strength reserve allows for the emergence and development of this coupling phenomenon. From the knowledge previously acquired from the authors, the strength curve to handle this specific type of L-D interaction must, ideally, have the following characteristics:

- I. Provide adequate failure load estimates for slender (L-D failures) and stocky (local failures) columns
- II. Lead to the NL curve for high R_{DL} values, *i.e.*, when the failure is purely local
- III. Fulfill the minimum LFRD resistance factor for compression members

Taking a close look at the NDL expression (Eq. (1)) it is possible to confirm that this design approach satisfies criterion II, since it leads to NL curve for high R_{DL} values (which yield low λ_{DL} values) – therefore, it is a candidate for handling SDB L-D interaction – the other criteria are addressed next. In an attempt to improve the estimates provided by the NDL approach, a new DSM-based design proposal is sought: the NSDB* approach. It is based on Eq. (7) and only differs in the third branch, *i.e.*, it is defined by (i) the NL curve, for $\lambda_L \leq \lambda_{L1}$, (ii) the NDL approach (the novelty), for $\lambda_L \geq \lambda_{L2}$, and (iii) a linear transition between the two previous branches (occurring in the $\Delta\lambda_L = \lambda_{L2} - \lambda_{L1}$ range) – it is expressed by

$$P_{nSDB^*} = \begin{cases} P_{nL} & , & \lambda_L \leq \lambda_{L1} \\ P_1 + \frac{P_2 - P_1}{\lambda_{L2} - \lambda_{L1}} (\lambda_L - \lambda_{L1}), & , & \lambda_{L1} < \lambda_L < \lambda_{L2} \\ P_{nDL} & , & \lambda_L \geq \lambda_{L2} \end{cases} \quad (10)$$

where the only distinct parameter is related to P_2 . It is now given by

$$P_2 = P_{nL_2} \lambda_{DL_2}^{-1.2} (1 - 0.25 \lambda_{DL_2}^{-1.2}) \quad \text{with} \quad P_{nL_2} = P_{y2} \lambda_{L_2}^{-0.8} (1 - 0.15 \lambda_{L_2}^{-0.8}) \quad \text{and} \quad \lambda_{DL_2} = \sqrt{\frac{P_{nL_2}}{P_{crD}}} \quad . \quad (10a)$$

Note that this design approach already accounts for the “border” between local ($\lambda_L \leq \lambda_{L1}$) and SDB L-D failures ($\lambda_L \geq \lambda_{L2}$) that was discussed in Section 2 – λ_{L1} is now defined by $\lambda_{L1} = 0.40R_{DL} + 0.60$, while λ_{L2} is still provided by $\lambda_{L1} + \Delta\lambda_L$.

In order to illustrate graphically (i) the difference between the NDL, NSDB* and NL approaches, and (ii) the evolution of the first two, as R_{DL} increases, Figs. 6(a)-(f) show the strength curves P_{nL}/P_y , P_{nDL}/P_y and P_{nSDB^*}/P_y vs. λ_L , for R_{DL} equal to 2.0, 3.0, 4.0, 6.0, 8.0 and 10.0, respectively. In addition, Figs. 6(a)-(f) also included show the numerical failure-to-yield load ratios P_U/P_y of the C, H, Z, R, WSLC and WFLC columns with the geometries given in Tables A.1 to A.6 of Appendix A – they exhibit 11 slenderness values ($\lambda_L = 1.0, 1.25, 1.50, 1.75, 2.0, 2.5, 3.0, 3.25, 3.50, 3.75, 4.0$) and, as mentioned in Section 2, contain critical-mode local initial geometrical imperfections. Figs. 7(a)-(e) display the von Mises stress contours of several failure modes (discussed below) and Figs. 8(a)-(b) show the P_{Exp}/P_{nDL} vs. λ_L and P_{Exp}/P_{nSDB^*} vs. λ_L plots for all the available experimental failure loads of columns susceptible to SDB L-D interaction – 70 specimens with C, R, WSLC and WFLC cross-sections (recall Table 1). As in the previous section, Figs. 9(a)-(f) and 10(a)-(f) show the P_U/P_{nDL} vs. λ_D and P_U/P_{nSDB^*} vs. λ_D plots¹⁴ concerning the numerical failure load ratios obtained (i) previously by Martins *et al.* (2015, 2016, 2017a) and (ii) in the current investigation, for $R_{DL} = 3.0, 4.0, 5.0, 6.0, 8.0, 10.0$ – as before, the values concerning the C, H, Z, R, WSLC

¹⁴The apparently “illogical” inclusion of the P_U/P_{nDL} and P_U/P_{nSDB^*} vs. λ_D plots in Figs. 9(a)-(f) and 10(a)-(f), instead of the more logical P_U/P_{nDL} and P_U/P_{nSDB^*} vs. λ_L ones, was intended to improve readability: because those values correspond to several pre-imposed local slenderness values ($\lambda_L = 1.00, \dots, 3.50$), they would be located on the same vertical line and, therefore, “on top of each other”.

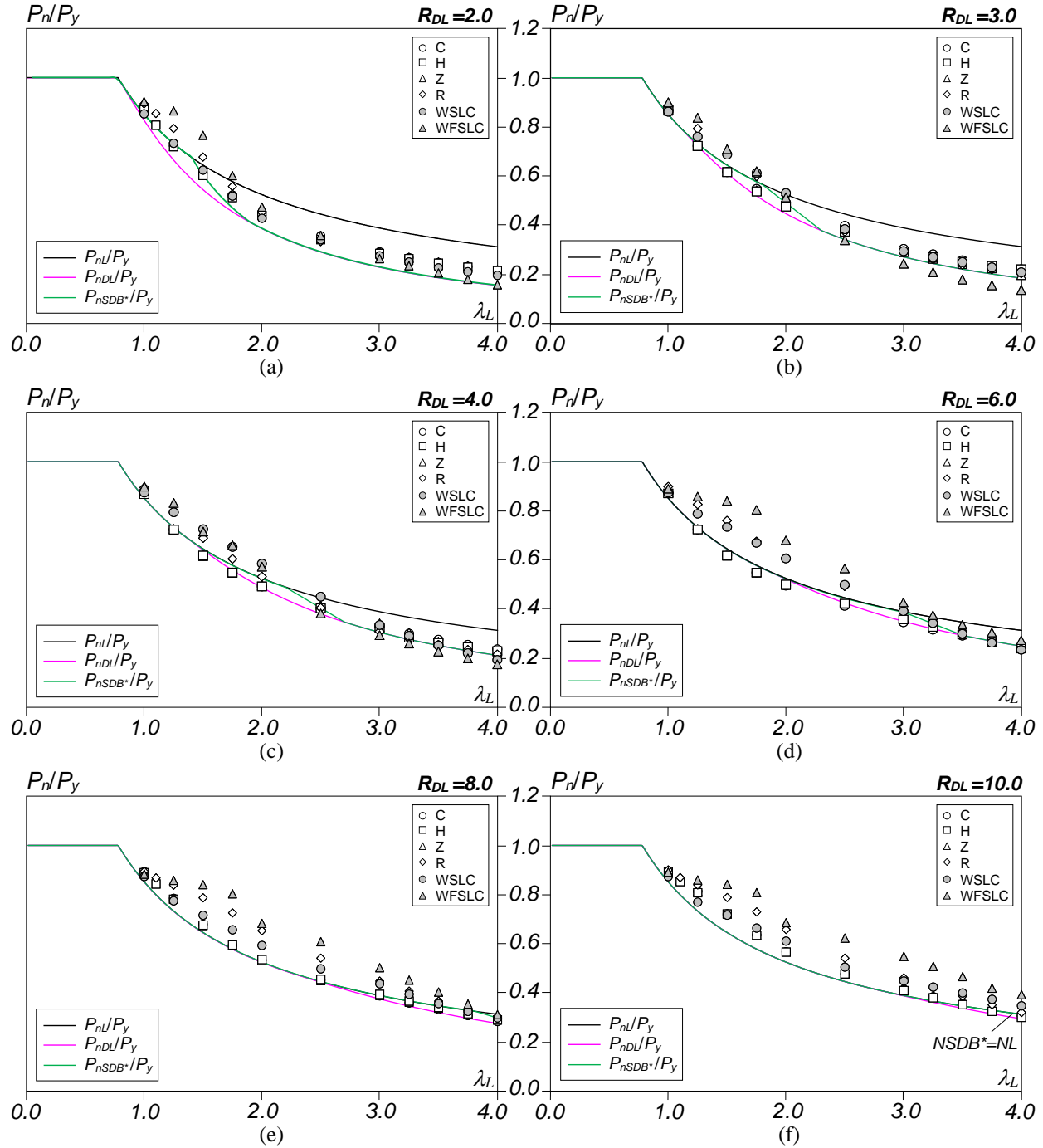


Figure 6: Plots of P_{nSDB^*}/P_y and P_{nDL}/P_y vs. λ_L with R_{DL} equal to (a) 2.0 (b) 3.0, (c) 4.0, (d) 6.0, (e) 8.0 and (f) 10.0

and WFSLC columns are plotted separately. In addition, Tables 4 and 5 provide the LFRD resistance factors obtained with the NDL and $NSDB^*$ estimates of the experimental and numerical failure loads, respectively. The observation of this set of results makes it possible to conclude that:

- (i) As mentioned before, Figs. 6(a)-(f) show that the NDL curve gradually approaches the NL curve as R_{DL} increases. Indeed, for $R_{DL}=10.0$ the NDL and NL curves practically coincide up to $\lambda_L=3.5$. Since it was shown that, for this buckling load ratio, the columns fail in pure local modes, regardless of the cross-section shape, the NDL approach is a valid candidate to also account for SDB L-D interaction.

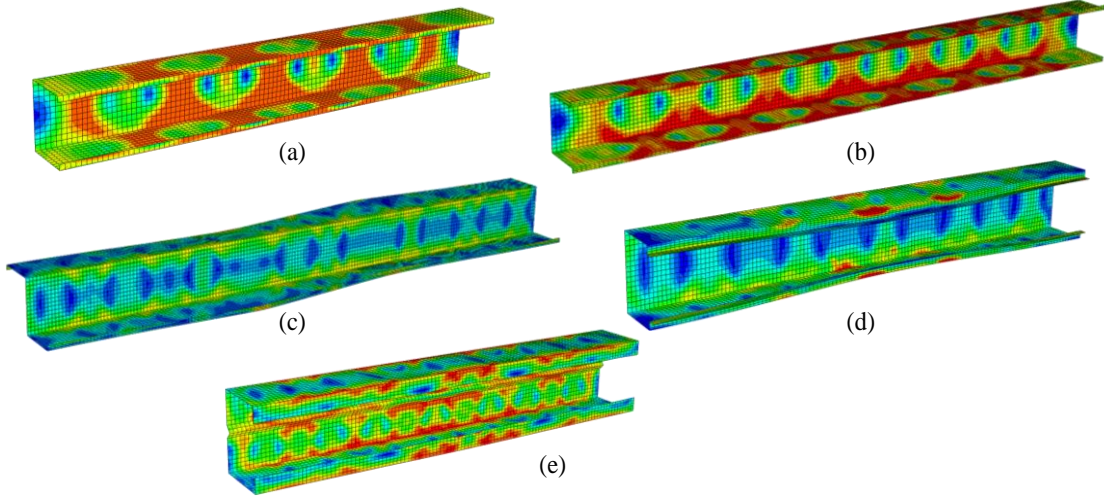


Figure 7: von Mises stress contours at the onset of collapse of the (a) $R_{DL}=2.0+\lambda_L=1.25$ C, (b) $R_{DL}=3.0+\lambda_L=1.75$ H, (c) $R_{DL}=3.0+\lambda_L=3.50$ Z, (d) $R_{DL}=6.0+\lambda_L=4.0$ R and (e) $R_{DL}=10.0+\lambda_L=4.0$ WSLC columns

Table 4: LRFD resistance factors ϕ according to AISI (2020) concerning the experimental failure loads of columns collapsing in secondary-distortional bifurcation interactive modes: NDL and NSDB* approaches

Cross-section	Reference	n	NDL				NSDB*			
			P_m	V_p	ϕ_1	ϕ_2	P_m	V_p	ϕ_1	ϕ_2
C	Loughlan <i>et al.</i> (2012)	20	1.30	0.08	1.15	1.31	1.26	0.11	1.08	1.22
C	Kwon <i>et al.</i> (2009)	5	0.91	0.11	0.72	0.82	0.85	0.15	0.62	0.70
C	Young <i>et al.</i> (2013)	16	1.02	0.05	0.93	1.06	0.99	0.07	0.89	1.01
R	Dinis <i>et al.</i> (2014)	10	1.01	0.03	0.92	1.05	1.01	0.03	0.92	1.05
C	Young & Rasmussen (1998)	3	1.07	0.11	0.74	0.83	1.05	0.09	0.80	0.90
WSLC	Kwon <i>et al.</i> (2009)	3	0.86	0.07	0.70	0.79	0.79	0.04	0.69	0.79
WSLC	He <i>et al.</i> (2014)	3	1.07	0.02	0.97	1.10	1.07	0.02	0.97	1.10
WFSLC	Yang & Hancock (2004)	4	0.92	0.06	0.79	0.90	0.92	0.06	0.79	0.90
WSLC	Chen <i>et al.</i> (2020)	4	1.12	0.03	1.01	1.15	1.12	0.03	1.01	1.15
WFSLC	Chen <i>et al.</i> (2020)	2	0.99	0.03	0.92	1.05	0.99	0.03	0.92	1.05
Total		70	1.09	0.15	0.90	1.01	1.06	0.16	0.86	0.98

- (ii) The analysis of the several column P_{Exp}/P_y ratios included in Figs. 6(a)-(f) shows that:
- (ii₁) The current local curve provides excellent estimates for the failure loads of stocky columns with low R_{DL} values (*e.g.*, $R_{DL}=2.0$ or 3.0) – the number of accurate estimates increases with R_{DL} . This is due to the fact that the columns effectively fail in local modes – Figs. 7(a)-(b) show the failure modes of two such columns ($R_{DL}=2.0+\lambda_L=1.25$ C and $R_{DL}=3.0+\lambda_L=1.75$ H columns).
 - (ii₂) The columns whose failure loads are not adequately estimated by the local strength curve are affected, to a smaller or larger extent, by SDB L-D interaction – *e.g.*, the $R_{DL}=2.0$ columns with $\lambda_L>2.0$ or $R_{DL}=3.0$ columns with $\lambda_L>2.5$ – Figs. 7(c)-(d) show the failure modes of two such columns ($R_{DL}=3.0+\lambda_L=3.50$ Z and $R_{DL}=6.0+\lambda_L=4.00$ R columns).
 - (ii₃) The failure mode transition, from local to SDB L-D interactive, as R_{DL} increases, is adequately captured by both the NSDB* (reflecting the content of Section 2) and NDL approaches.
 - (ii₄) For high R_{DL} values (*e.g.*, 8.0 and 10.0), the three design approaches practically coincide for the whole slenderness range. It is observed that all the $R_{DL}=10.0$ columns fail in local modes, up to $\lambda_L=4.0$ – Fig. 7(e) shows the failure mode of one such column ($R_{DL}=10.0+\lambda_L=4.00$ WSLC).
 - (ii₅) In view of the contents of the previous sub-items, it can be concluded that criteria I and II are fulfilled by both the NSDB* and NDL design approaches. Criterion III is assessed next.

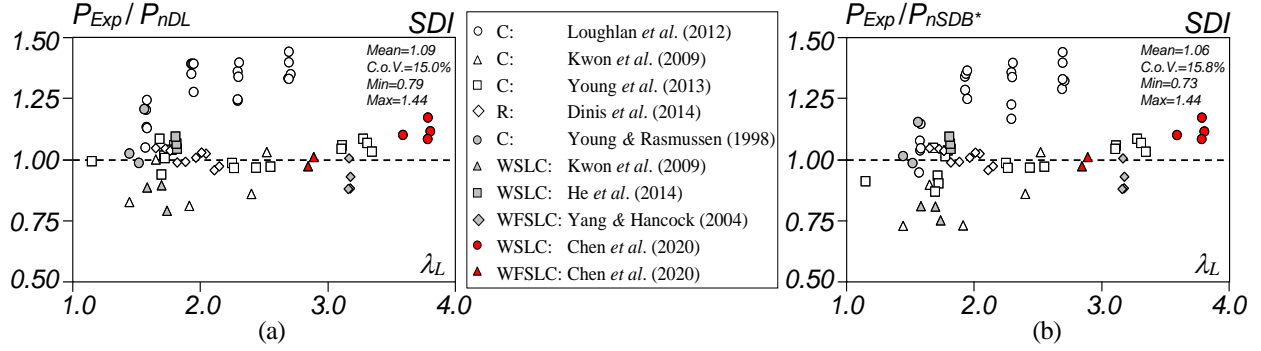


Figure 8: Plots (a) P_{Exp}/P_{nDL} and (b) P_{Exp}/P_{nSDB^*} vs. λ_L concerning the available experimental failure loads of columns collapsing in secondary-distortional bifurcation L-D interactive modes

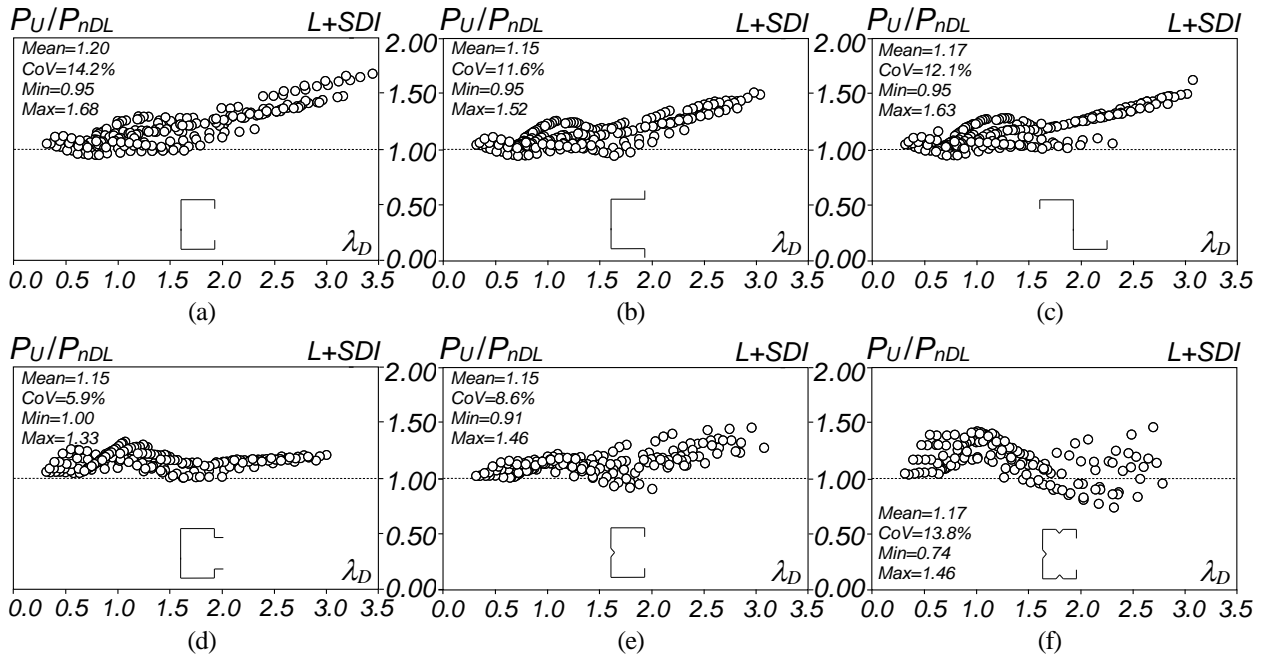


Figure 9: Plots P_U/P_{nDL} vs. λ_D for the numerical failure loads of columns collapsing in local and secondary-distortional bifurcation L-D interactive modes: (a) C, (b) H, (c) Z, (d) R, (e) WSLC and (f) WFSLC columns

(iii) Concerning the experimental failure load prediction of columns prone to SDB L-D interaction (see Figs 8(a)-(b) and Table 4), it is clear that it is adequately handled by the two design approaches, as they provide LFRD resistance factors higher than the value prescribed in AISI (2020): $\phi_l=0.90$ (NDL) vs. $\phi_l=0.86$ (NSDB*) or $\phi_2=1.01$ (NDL) vs. $\phi_2=0.98$ (NSDB*) if $M_m=1.192$ and $V_M=0.031$ are adopted. As in Section 4.2, the failure loads reported by Kwon *et al.* (2005, 2009) are the most underestimated. Conversely, the failure loads reported by Loughlan *et al.* (2012) are the most overestimated since they correspond to failures occurring in the transition between local and SDB L-D interaction – even if the NSDB* approach yields failure load estimates closer to the NL ones than its NDL counterpart, the fact that a conservative estimate of that border was used (see Section 2) prevents a more accurate assessment of these results. Nonetheless, and generally speaking, very good means and CoVs were obtained for the experimental-to-predicted load ratios of both approaches: 1.09 and 15% vs. 1.06 and 16%, for the NDL and NSDB* approaches, respectively.

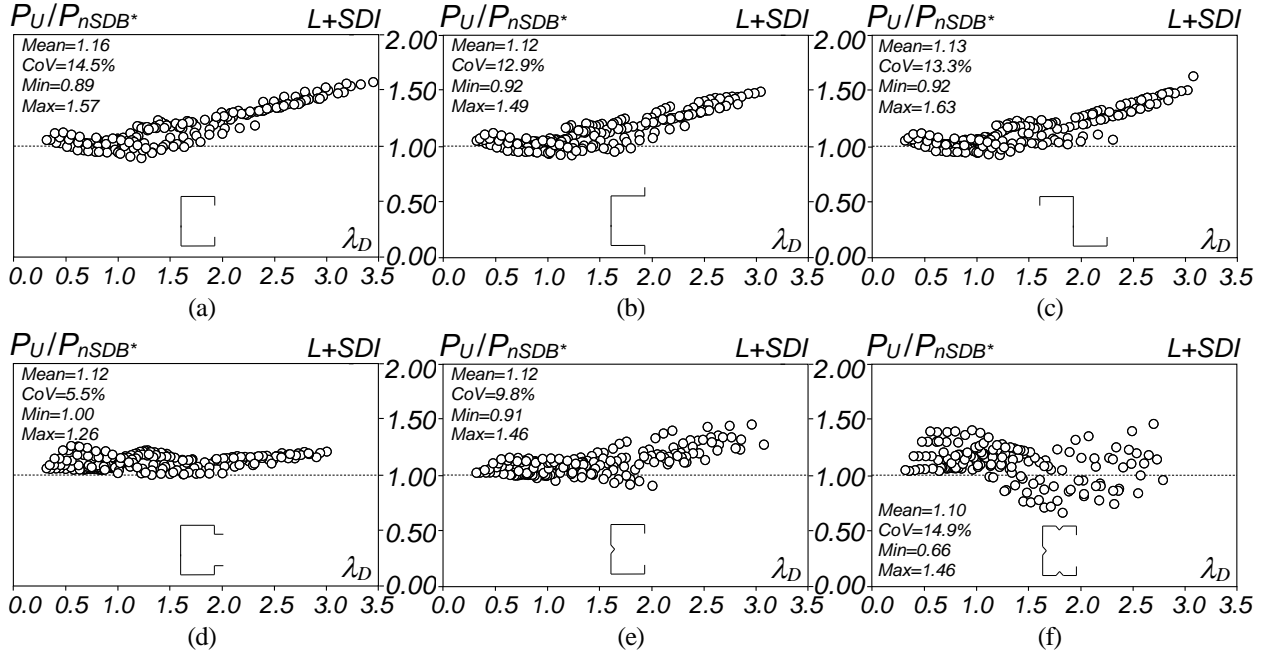


Figure 10: Plots P_U/P_{nSDB^*} vs. λ_D for the numerical failure loads of columns collapsing in local and secondary-distortional bifurcation L-D interactive modes: (a) C, (b) H, (c) Z, (d) R, (e) WSLC and (f) WFSLC columns

Table 5: LFRD resistance factors ϕ according to AISI (2020) concerning the numerical failure loads of columns collapsing in local and secondary-distortional bifurcation L-D interactive modes: NDL and NSDB* approaches

Cross-section	Source	n	NDL			NSDB*		
			P_m	V_p	ϕ_I	P_m	V_p	ϕ_I
C	Martins <i>et al.</i> (2015) + Dinis & Camotim (2015) + current work	197	1.20	0.14	1.00	1.16	0.14	0.96
H	Martins <i>et al.</i> (2015) + Dinis & Camotim (2015) + current work	204	1.15	0.12	0.99	1.12	0.13	0.95
Z	Martins <i>et al.</i> (2015) + Dinis & Camotim (2015) + current work	204	1.17	0.12	1.00	1.13	0.13	0.95
R	Martins <i>et al.</i> (2015) + Dinis & Camotim (2015) + current work	194	1.15	0.06	1.04	1.12	0.05	1.01
WSLC	Martins <i>et al.</i> (2016) + current work	176	1.15	0.09	1.02	1.12	0.10	0.98
WFSLC	Martins <i>et al.</i> (2017a) + current work	155	1.17	0.14	0.98	1.10	0.15	0.91
Total		1130	1.17	0.11	1.01	1.12	0.12	0.96

(iv) The comparison between the numerically-based P_U/P_{nDL} vs. λ_D and P_U/P_{nSDB^*} vs. λ_D plots presented in Figs. 9(a)-(f) and 10(a)-(f) shows a clear resemblance between the corresponding clouds of points. These figures also show that both design approaches perform very well, in the whole slenderness range, for R and WSLC columns. For the remaining columns, there is a noticeable overestimation for $\lambda_D > 2.0$, occurring mainly for the columns with $1.30 < R_{DL} < 2.40$. As for the experimental failure loads, the NSDB* approach also performs slightly better than its NDL counterpart: similar CoVs and averages closer to 1.0. Similar conclusions can be drawn from Table 5 – indeed, the two LFRD resistance factors are very close for each column cross-section (the NSDB* values are a bit lower) and always above the minimum value ($\phi_t = 0.85$) recommended in AISI (2020).

(v) The WFSLC column results differ significantly from those concerning the columns with other cross-section shapes. Indeed, such columns were found to exhibit (v_1) much higher local post-critical

strengths and, conversely, (v_2) visibly lower distortional post-critical strengths (see also Section 4.4) than the columns with the other cross-section shapes. Thus, in WFSLC columns with $R_{DL}>1.30$ (those experiencing SDB L-D interaction), the emergence of distortional deformations causes a rapid strength erosion, as clearly noticeable in Figs. 6(a)-(f). This behavioral feature leads to large failure load overestimations in columns failing in local modes (P_U/P_{nDL} or P_U/P_{nSDB^*} ratios visibly above 1.0 – see Figs. 9(f) and 10(f)) and P_U/P_{nDL} or P_U/P_{nSDB^*} ratios close or a bit below 1.0 in columns failing in SDB L-D interactive modes. This feature also increases the P_U/P_{nDL} and P_U/P_{nSDB^*} COVs, thus affecting negatively the LFRD resistance factors – nevertheless, they still remain well above the minimum value prescribed by AISI (2020): $\phi_I=0.98$ (NDL) or $\phi_I=0.91$ (NSDB^{*}) – see Table 5.

- (vi) Finally, on the basis of the findings presented it may be argued that the NDL and NSDB^{*} design approaches can handle adequately columns with $R_{DL}>1.30$ columns, since both of them fulfill the three criteria mentioned earlier. Even if the latter performs slightly better, it seems is preferable to propose the NDL approach, for the sake of generality and simplicity – recall that the NDL approach has already been shown to also handle adequately columns prone to True L-D interaction, which means that a single DSM-based design approach can be used to predict the failure loads of columns collapsing in TI and SDB L-D interactive modes (and also in local modes).

4.4 Secondary-Local Bifurcation L-D Interaction

It is by now well known that the moderate¹⁵ distortional post-critical strength reserve, typical of most CFS columns, precludes significant failure load erosion, with respect to the failure load estimate provided by the currently codified distortional design curve (ND), caused by SLB L-D interaction. The validity of this assertion is assessed next, using the numerical failure load data obtained in past investigations involving columns with $R_{DL}<0.80$. As mentioned in Section 2, the columns undergoing SLB L-D interaction are, approximately and conservatively, those for which $\lambda_D>2.44-1.6P_{crD}/P_{crL}$.

Like in the previous sections, Figs. 11(a)-(f) show plots P_U/P_{nD} vs. λ_L ¹⁶ for the available numerical failure loads, concerning columns with six cross-section shapes, while Table 6 provides the corresponding statistical indicators (average, CoV, minimum and maximum values). With the exception of the WFSLC columns (discussed below), these results confirm that the current ND curve handles adequately CFS columns affected by SLB L-D interaction, due to the negligible failure load erosion involved. Indeed, the P_U/P_{nD} exhibit means barely exceeding 1.0 and CoVs never exceeding 7.0%, which leads to resistance factors very close to 1.00, *i.e.*, significantly above the minimum value ($\phi_t=0.85$) prescribed by AISI (2020). However, while the C, H, Z, R, WSLC column P_U/P_{nD} values are grouped in quite similar “clouds”, those concerning the WFSLC columns are clearly different: they decrease almost linearly with λ_L and fall below 1.0 for $\lambda_L>2.0$. This behavior is not due a severe interaction – instead, it stems from the very low distortional post-critical strength of the WFSLC columns (much lower than for the columns with other cross-section shapes), which is probably associated with the presence of flange stiffeners. This fact leads to lower P_U/P_{nD} ratios for the most slender columns, *i.e.*, those more susceptible to L-D interaction. This behavioral feature, responsible for a resistance factor a bit below the minimum value prescribed in AISI (2020) ($\phi_I=0.81<0.85$), is caused by the (logical) inability of the current ND curve to accommodate all possible distortional post-critical strengths in a single expression (depending only on λ_D).

Turning the attention now to the experimental failure loads, Table 1 shows that only 6 specimens fall into this category: 1 tested by Kwon & Hancock (1992) and 5 tested by Yap & Hancock (2011). Concerning

¹⁵When compared with its local post-critical counterpart.

¹⁶See footnote 14, whose content is now applied to λ_D .

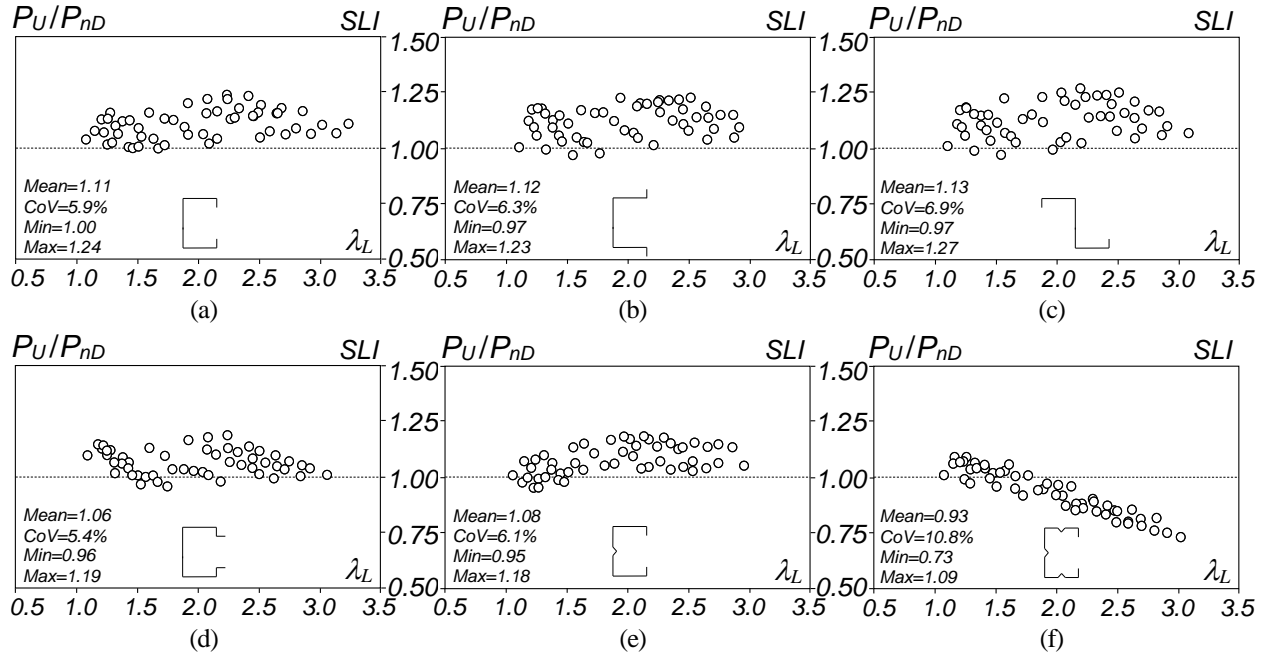


Figure 11: Plots P_U/P_{nD} vs. λ_L for the numerical failure loads of the columns undergoing secondary-local bifurcation L-D interaction: (a) C, (b) H, (c) Z, (d) R, (e) WSLC and (f) WFSLC columns

Table 6: LRFD resistance factors ϕ according to AISI (2020) concerning the numerical failure loads of the columns undergoing secondary-local bifurcation L-D interaction: ND approach

Cross-section	Source	ND			
		n	P_m	V_p	ϕ_I
C	Martins <i>et al.</i> (2015)	54	1.11	0.06	1.00
H	Martins <i>et al.</i> (2015)	52	1.12	0.06	1.01
Z	Martins <i>et al.</i> (2015)	51	1.13	0.07	1.01
R	Martins <i>et al.</i> (2015)	52	1.06	0.05	0.96
WSLC	Martins <i>et al.</i> (2016)	51	1.08	0.06	0.97
WFSLC	Martins <i>et al.</i> (2017a)	52	0.93	0.11	0.81
Total		312	1.07	0.09	0.94

the first specimen, the currently codified distortional design curve predicts adequately its failure load, ($P_{Exp}/P_{nD}=1.13$). Regarding the remaining 5 specimens, an in-depth examination of Yap's Ph.D. thesis (Yap 2008), which is much more detailed than the paper of Yap & Hancock (2011), strongly indicates that their failure loads are not eroded by SLB L-D interaction. In fact, photos and failure loads included in this thesis provide evidence that these specimens failed in distortional modes and local deformations (barely visible in the photos) only appeared after the peak load had been reached. Nonetheless, it is worth noting that these failure loads are not accurately predicted by the current distortional (ND) design curve. This feature was previously reported by Landesmann *et al.* (2016) and Martins *et al.* (2017b), who (i) attributed the failure load overestimations to the joint influence of the (i) cross-section dimensions (particularly the b_f/b_l ratio) and (ii) critical distortional buckling mode half-wave number n_D , and (ii) recommended the development of a new distortional design curve able to adequately account for the dependence of the failure load on b_f/b_l and n_D (and not only on λ_D).

4.5 Summary

This section summarizes the DSM-based design approach proposed for CFS columns undergoing L-D interaction, termed “NL-D approach”¹⁷, which covers the three L-D interaction types identified earlier:

- SLB L-D interaction ($P_{crD}/P_{crL} < 0.80$): $P_{nL-D} = P_{nD}$
- TIL-D interaction and SDB L-D interaction ($1.30 \leq P_{crD}/P_{crL} \leq 0.80$ and $P_{crD}/P_{crL} \geq 1.30$): $P_{nL-D} = P_{nDL}$

In order to avoid a discontinuity at $P_{crD}/P_{crL} = 0.80$, it is proposed a (conservative) linear transition between $P_{crD}/P_{crL} = 0.70$ and $P_{crD}/P_{crL} = 0.80$, *i.e.*, the joint DSM-based design approach accounting the three L-D interaction types is defined by

$$P_{nL-D} = \begin{cases} P_{nD}, & \frac{P_{crD}}{P_{crL}} \leq 0.70 \\ P_{nD} - \left(\frac{P_{nD} - P_{nDL}}{0.10} \right) \left(\frac{P_{crD}}{P_{crL}} - 0.70 \right), & 0.70 < \frac{P_{crD}}{P_{crL}} < 0.80 \\ P_{nDL}, & \frac{P_{crD}}{P_{crL}} \geq 0.80 \end{cases} \quad (11)$$

where P_{nD} and P_{nDL} have already been defined in Eqs. (4) and (1), respectively.

For illustrative purposes, Figs. 12(a)-(c) show graphical representations of the proposed DSM-based design approach (P_{nL-D}/P_y vs. λ_D or λ_L) for columns with P_{crD}/P_{crL} values belonging to each Eq. (11) branch, *i.e.*, columns with (i) $P_{crD}/P_{crL} < 0.70$, (ii) $P_{crD}/P_{crL} = 0.75$ and (iii) $P_{crD}/P_{crL} = 1.0, 2.5, 5.0$ and 7.5 .

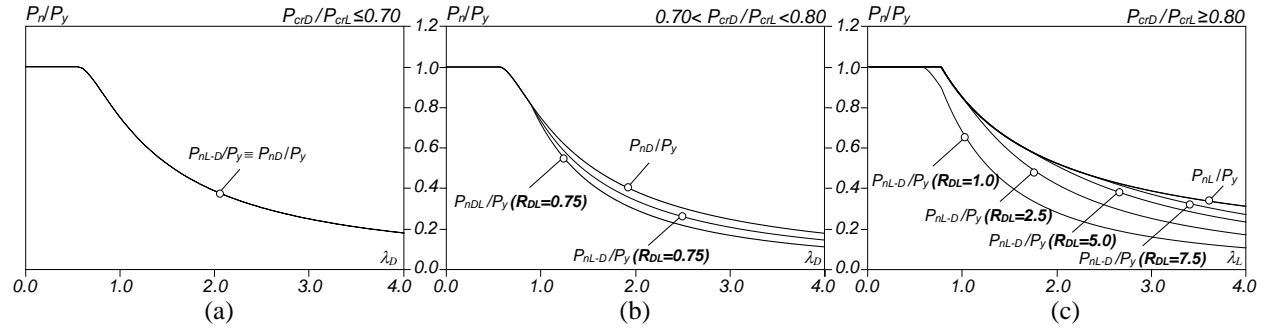


Figure 12: Graphical representation of the proposed DSM-based design approach for columns affected by L-D interaction with (a) $P_{crD}/P_{crL} \leq 0.70$, (b) $0.70 < P_{crD}/P_{crL} < 0.80$, and (c) $P_{crD}/P_{crL} \geq 0.80$

5. Concluding Remarks

This work addressed the development and proposal of a rational and efficient (accurate, safe and reliable) design approach, based on the Direct Strength Method (DSM), for cold-formed steel (CFS) columns experiencing L-D interaction, a coupling phenomenon relevant in short-to-intermediate columns. This design approach, believed to be ready for codification, was developed mainly on the basis of the available experimental failure loads corresponding to clear L-D interactive modes, thus preserving the philosophy adopted for other limit states currently covered by the DSM – nevertheless, a sizeable amount of numerical failure loads were also considered when developing the design approach. The experimental and numerical failure load data involving almost exclusively columns (i) with six commonly used CFS cross-section shapes, namely lipped channels (C), hat-sections (H), zed-sections (Z), rack-sections (R), web-stiffened lipped channels (WSLC) and web-flange-stiffened lipped channels (WFSLC), and (ii)

¹⁷To avoid confusion with the NLD and NDL approaches defined in Eqs. (1-2).

affected by three types of L-D interaction, namely (ii₁) true L-D interaction ($0.80 \leq P_{crD}/P_{crL} \leq 1.30$), (ii₂) secondary-distortional bifurcation L-D interaction ($SDI - P_{crD}/P_{crL} > 1.30$), and (ii₃) secondary-local bifurcation L-D interaction ($SLI - P_{crD}/P_{crL} < 0.80$).

The paper begins with the determination of approximate borders separating the columns failing (i) in local and SDB L-D interactive modes, and (ii) in distortional and SLB L-D interactive modes, based exclusively on numerical failure load data. The first border played a crucial role in the development of a new DSM-based design approach to handle SDB L-D interactive failures – (NSDB* approach). Then, the available experimental L-D interactive failure load data, involving 161 C, H, R, WSLC, WFLC and CSCS (complex-stiffened cross-sections) specimens tested by several researchers worldwide over a period of about 30 years, were collected and characterized. Next, after reviewing the existing DSM-based design approaches to handle column L-D interactive failures, the paper addressed those developed to handle TI and SDB L-D interactive failures – their merits were assessed through the quality of the experimental (mostly) and numerical failure load predictions and the LFRD resistance factors they lead to, which should not be below the minimum value prescribed in AISI (2020) for compression members ($\phi_c=0.85$). For columns undergoing SLI L-D interaction, which experience very little failure load erosion due to L-D interaction, it was found that the currently codified DSM distortional design (ND) curve provides accurate failure load predictions.

Concerning the columns undergoing TI L-D interaction, it was found that the ND approach is able to predict quite adequately the experimental failure data, leading to LFRD resistance factors significantly above the minimum value prescribed – it also provides mostly conservative estimates of the numerical failure loads. Regarding the columns undergoing SDB L-D interaction, the ND and NSDB* DSM-based design approaches were found to satisfy the three criteria deemed to ensure an efficient design approach, namely (i) L-D interactive failure load prediction accuracy, (ii) smooth transition to the current NL as $R_{DL}=P_{crD}/P_{crL}$ increases and the slenderness decreases, and (iii) LFRD resistance factors exceeding the minimum values prescribed in AISI (2020) for compression members. Although the NSDB* approach performed slightly better, generality and simplicity led to the choice of the ND approach, which then was proposed to handle the TI and SDB L-D interactive failures (and also local ones) of columns with $P_{crD}/P_{crL} > 0.80$. However, in order to avoid a abrupt failure load prediction in the vicinity of $P_{crD}/P_{crL} = 0.80$ (recall that the current ND design curve is to be applied when $P_{crD}/P_{crL} < 0.80$), it was decided to propose a linear transition between the ND and ND approach for columns in the $0.70 < P_{crD}/P_{crL} < 0.80$ range, to avoid a steep/abrupt strength variation at the vicinity of $P_{crD}/P_{crL} = 0.80$.

Finally, a few words to mention that, obviously, the presence of L-D interaction does not benefit the CFS industry, since it may lead to a significant failure load erosion. However, the knowledge about this coupling phenomenon acquired provides appropriate tools for designers to avoid its occurrence (*e.g.*, through small changes in the cross-section dimensions or appropriate stiffeners). If such avoidance is not possible (*e.g.*, due to architectural constraints), this limit state must be taken into account by means of the design approach proposed in this work – otherwise, unsafe designs can be reached. At the moment, the nominal strength of a CFS column (P_n) is given by $P_n = \min\{P_{nL}, P_{nD}, P_{nG}, P_{nLG}\}$ and it is proposed here to change this condition to $P_n = \min\{P_{nL}, P_{nD}, P_{nG}, P_{nLG}, P_{nL-D}\}$, by adding the safety check against L-D interactive failures. In order to reach a fully safe design of CFS columns, particularly those made of high-strength steel, it is indispensable to add safety checks against the interactive failures still unaccounted for, namely distortional-global (D-G), local-distortional-global (L-D-G) and global-global (G-G) failures. Although research work towards achieving this goal has been under way for a number of years (*e.g.*, Martins *et al.* 2018b, Young *et al.* 2018, Dinis *et al.* 2018, 2022), DSM-based design approaches that can be considered for codification are still missing, mostly due to the lack of adequate experimental evidence.

References

- AISI (American Iron and Steel Institute) (2020). *North American Specification (NAS) for the Design of Cold-Formed Steel Structural Members* (2016 edition reaffirmed in 2020), AISI-S100-16 w/S2-20, Washington DC.
- Bebiano, R., Camotim, D., Gonçalves, R. (2018). “GBTUL 2.0 – a second-generation code for the GBT-based buckling and vibration analysis of thin-walled members”, *Thin-Walled Structures*, 124(March), 235-257.
- Camotim, D., Dinis, P.B., Martins, A.D. (2016). “Direct Strength Method (DSM) – a general approach for the design of cold-formed steel structures”, *Recent Trends in Cold-Formed Steel Construction*, C. Yu (ed.), Woodhead Publishing (Series in Civil and Structural Engineering), Amsterdam, 69-105.
- Chen, J., Chen, M.-T., Young, B. (2019). “Compression tests of cold-formed steel C- and Z-sections with different stiffeners”, *Journal of Structural Engineering* (ASCE), 145(5), 04019022 (10 pages).
- Chen, M.-T., Young, B., Martins, A.D., Camotim, D., Dinis, P.B. (2020). “Experimental investigation on cold-formed steel stiffened lipped channel columns undergoing local-distortional interaction”, *Thin-Walled Structures*, 150(May), 106682 (20 pages).
- Dinis, P.B., Young, B., Camotim, D. (2014a). “Local-distortional interaction in cold-formed steel rack-section columns”, *Thin-Walled Structures*, 81(August), 185-194.
- Dinis, P.B., Young, B., Camotim, D. (2014b). “Strength, interactive failure and design of web-stiffened lipped channel columns exhibiting distortional buckling”, *Thin-Walled Structures*, 81(August), 195-209.
- Dinis, P.B., Camotim, D., Young, B., Batista, E.M. (2018). “CFS lipped channel columns affected by L-D-G interaction – Part II: Numerical simulations and design Considerations”, *Computers & Structures*, 207(September), 200-218.
- Dinis, P.B., Camotim, D., Landesmann, A., Martins, A.D., Cerqueira, E. (2022). “Global-global Interaction in cold-formed steel plain and lipped channel columns”, *Thin-Walled Structures*, in press, 2022.
- Dinis, P.B., Camotim, D. (2015). “Cold-formed steel columns undergoing local-distortional coupling: behaviour and direct strength prediction against interactive failure”, *Computers & Structures*, 147(January), 181-208.
- He, Z., Zhou, X., Liu, Z., Chen, M. (2014). “Post-buckling behaviour and DSM design of web-stiffened lipped channel columns with distortional and local mode interaction”, *Thin-Walled Structures*, 84(November), 189-203.
- Hsiao, L.-E. (1989). “Reliability based criteria for cold-formed steel members”, PhD. Thesis, University of Missouri-Rolla.
- Hsiao, L.-E., Yu, W.W., Galambos, T.V. (1988). “Load and resistance factor design of cold-formed steel: comparative study of design methods for cold-formed steel”, 11th Progress Report, Civil Engineering Study 88-4, University of Missouri-Rolla.
- Kwon, Y.B., Hancock, G.J. (1992). “Tests of cold-formed channels with local and distortional buckling”, *Journal of Structural Engineering* (ASCE), 118(7), 1786-1803.
- Kwon, Y.B., Kim, B.S., Hancock, G.J. (2009). “Compression tests of high strength cold-formed steel channel with buckling interaction”, *Journal of Constructional Steel Research*, 65(2), 278-289.
- Kwon, Y.B., Kim, N.K., Kim, B.S. (2005). “A study on the direct strength method for compression members undergoing mixed mode buckling”, *Proceedings of 3rd International Symposium on Steel Structures (ISSS’05 – Seoul 10-11/03)*, 108-119.
- Landesmann, A., Camotim, D., Garcia, R. (2016). “On the strength and DSM design of cold-formed steel web/flange-stiffened lipped channel columns buckling and failing in distortional modes”, *Thin-Walled Structures*, 105(August), 248-265.
- Loughlan, J., Yidris, N., Jones, K. (2012). “The failure of thin-walled lipped channel compression members due to coupled local-distortional interactions and material yielding”, *Thin-Walled Structures*, 61(December), 14-21.
- Martins, A.D., Dinis, P.B., Camotim, D., Providência, P. (2015). “On the relevance of local-distortional interaction effects in the behaviour and design of cold-formed steel columns”, *Computers & Structures*, 160(November), 57-89.
- Martins, A.D., Dinis, P.B., Camotim, D. (2016). “On the influence of local-distortional interaction in the behaviour and design of cold-formed steel web-stiffened lipped channel columns”, *Thin-Walled Structures*, 101(April), 181-204.
- Martins, A.D., Camotim, D., Dinis, P.B. (2017a). “Behaviour and DSM design of stiffened lipped channel columns undergoing local-distortional interaction”, *Journal of Constructional Steel Research*, 128(January), 99-118.
- Martins, A.D., Camotim, D., Dinis, P.B. (2017b). “On the direct strength design of cold-formed steel columns failing in local-distortional interactive modes”, *Thin-Walled Structures*, 120(November), 432-445.
- Martins, A.D., Camotim, D., Gonçalves, R., Dinis, P.B. (2018a). “On the mechanics of local-distortional interaction in thin-walled lipped channel columns”, *Thin-Walled Structures*, 125(April), 187-202.
- Martins, A.D., Camotim, D., Dinis, P.B. (2018b). “On the distortional-global interaction in cold-formed steel columns: relevance, post-buckling behaviour, strength and DSM Design”, *Journal of Constructional Steel Research*, 145(June), 449-470.
- Matsubara, G.Y., Batista, E.M., Salles, G.C. (2019). “Lipped channel cold-formed steel columns under local-distortional buckling mode interaction”, *Thin-Walled Structures*, 137(April), 251-270.
- Pham, C.H., Hancock, G.J. (2012). “Direct strength design of cold-formed c-sections for shear and combined actions”, *Journal of Structural Engineering* (ASCE), 138(6), 759-768.
- Prola, L.C., Camotim, D. (2002). “On the distortional post-buckling behaviour of cold-formed lipped channel steel columns”, *Proceedings of Structural Stability Research Council Annual Stability Conference* (Seattle, 24-27/4), 571-590.

- Schafer, B.W. (2002). “Local, distortional and Euler buckling in thin-walled columns”, *Journal of Structural Engineering* (ASCE), 128(3), 289-299.
- Schafer BW (2008). Review: the direct strength method of cold-formed steel member design, *Journal of Constructional Steel Research*, 64(7-8), 766-778.
- Schafer, B.W. (2019). “Advances in the Direct Strength Method of cold-formed steel design”, *Thin-Walled Structures*, 140(July), 533-541.
- Silvestre, N., Camotim, D., Dinis, P.B. (2009). “Direct strength prediction of lipped channel columns experiencing local-plate/distortional interaction”, *Advanced Steel Construction*, 5(1), 49-71.
- Silvestre, N., Camotim, D., Dinis, P.B. (2012). “Post-buckling behaviour and direct strength design of lipped channel columns experiencing local/distortional interaction”, *Journal of Constructional Steel Research*, 73(June), 12-30.
- Simulia Inc. (2008), *ABAQUS Standard* (version 6.7-5).
- Yang, D., Hancock, G.J. (2004). “Compression tests of high strength steel channel columns with interaction between local and distortional buckling”, *Journal of Structural Engineering* (ASCE), 130(12), 1954-1963.
- Yap, D.C.Y. (2008). “Local and Distortional Buckling of High Strength Cold-Formed Steel Sections”, Ph.D. Thesis, School of Civil Engineering, University of Sydney, Australia.
- Yap, D.C.Y., Hancock, G.J. (2006). “Compression tests of high strength cold-formed cross-shaped steel columns”, *Research Report N° R869*, School of Civil Engineering, University of Sydney, Australia.
- Yap, D.C.Y., Hancock, G.J. (2011). “Experimental study of high strength cold-formed stiffened-web C-sections in compression”, *Journal of Structural Engineering* (ASCE), 137(2), 162-172.
- Yap, D.C.Y., Hancock, G.J. (2008). “Experimental study of complex high-strength cold-formed cross-shaped steel section”, *Journal of Structural Engineering* (ASCE), 134(8), 1322-1333.
- Young, B., Rasmussen, K.J.R. (1998). “Design of lipped channel columns”, *Journal of Structural Engineering* (ASCE), 124(2), 140-148.
- Young, B., Silvestre, N., Camotim, D. (2013). “Cold-formed steel lipped channel columns influenced by local-distortional interaction: strength and DSM design”, *Journal of Structural Engineering* (ASCE), 139(6), 1059-1074.
- Young, B., Dinis, P.B., Camotim, D. (2018). “CFS lipped channel columns affected by L-D-G interaction – Part I: Experimental investigation”, *Computers & Structures*, 207(September), 219-232.

Appendix A – Additional column geometries considered

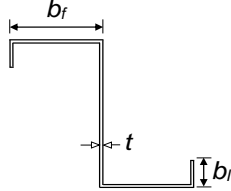
Table A.1: Lipped channel columns: geometries, critical distortional and local buckling stresses and relevant buckling stress/load ratios (dimensions in *mm* and stresses in *MPa*)

Column	b_w	b_f	b_l	t	L	f_{crD}	f_{crL}	R_{DL}	f_{crG}/f_{crD}
C1	120	100	10	0.4870	1500	45.8	15.3	3.00	25.1
C2	120	100	10	0.4420	1200	50.4	12.6	4.00	35.7
C3	120	100	10	0.4460	1000	64.2	12.8	5.00	40.4
C4	120	100	10	0.4015	1000	62.5	10.4	6.00	41.5
C5	130	90	10	0.4050	900	77.3	9.7	8.00	46.1
C6	120	75	12	0.4760	800	160.2	16.0	10.0	24.3

Table A.2: Hat-section columns: geometries, critical distortional and local buckling stresses and relevant buckling stress/load ratios (dimensions in *mm* and stresses in *MPa*)

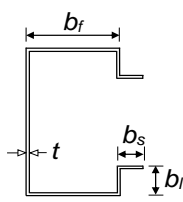
Column	b_w	b_f	b_l	t	L	f_{crD}	f_{crL}	R_{DL}	f_{crG}/f_{crD}
H1	120	100	10	0.4910	1500	46.7	15.5	3.00	21.4
H2	120	100	10	0.4451	1200	51.2	12.8	4.00	30.6
H3	120	100	10	0.4490	1000	65.1	13.0	5.00	34.6
H4	120	100	10	0.4040	1000	63.3	10.5	6.00	35.6
H5	130	90	10	0.4091	900	78.9	9.9	8.00	39.2
H6	120	75	12	0.4860	800	166.9	16.7	10.0	18.4

Table A.3: Lipped zed-section columns: geometries, critical distortional and local buckling stresses and relevant buckling stress/load ratios (dimensions in *mm* and stresses in *MPa*)



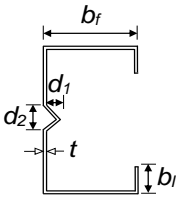
Column	b_w	b_f	b_l	t	L	f_{crD}	f_{crL}	R_{DL}	f_{crG}/f_{crD}
Z1	120	100	10	0.4890	1500	46.3	15.4	3.00	43.4
Z2	120	100	10	0.4420	1200	50.4	12.6	4.00	62.2
Z3	120	100	10	0.4450	1000	64.0	12.8	5.00	70.6
Z4	120	100	10	0.4005	1000	62.2	10.4	6.00	72.6
Z5	130	90	10	0.4030	900	76.6	9.6	8.00	69.4
Z6	120	75	12	0.4728	800	158.0	15.8	10.0	33.1

Table A.4: Rack-section columns: geometries, critical distortional and local buckling stresses and relevant buckling stress/load ratios (dimensions in *mm* and stresses in *MPa*)



Column	b_w	b_f	b_{l1}	b_{l2}	t	L	f_{crD}	f_{crL}	R_{DL}	f_{crG}/f_{crD}
R1	130	100	15	15	1.160	1200	237.2	79.0	3.00	10.8
R2	130	100	15	15	1.138	1000	305.1	76.3	4.00	12.1
R3	140	90	15	15	1.054	1000	292.3	58.4	5.00	13.8
R4	140	90	15	15	0.950	1000	285.1	47.5	6.00	14.2
R5	140	80	15	15	0.866	900	321.5	40.2	8.00	15.1
R6	140	80	15	15	0.856	800	394.0	39.4	10.0	15.6

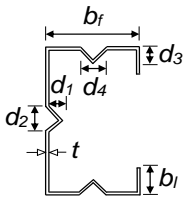
Table A.5: Web-stiffened lipped channel columns: geometries, critical distortional and local buckling stresses and relevant buckling stress/load ratios (dimensions in *mm* and stresses in *MPa*)



Column	b_w	b_f	b_l	t	L	f_{crD}	f_{crL}	R_{DL}	f_{crG}/f_{crD}
WSLC1	160	120	12.5	0.8420	800	141.2	47.0	3.00	50.2
WSLC2	160	110	20	0.5100	2000	82.4	20.6	4.00	14.7
WSLC3	160	110	20	0.4385	2000	76.1	15.2	5.00	15.9
WSLC4	150	110	20	0.4660	1600	103.4	17.2	6.00	16.6
WSLC5	140	100	25	0.4475	1200	153.4	19.2	8.00	19.1
WSLC6	130	100	25	0.4740	800	216.4	21.6	10.0	27.5

*in all columns, $d_1=10$ and $d_2=20$ mm.

Table A.6: Web-flange-stiffened lipped channel columns: geometries, critical distortional and local buckling stresses and relevant buckling stress/load ratios (dimensions in *mm* and stresses in *MPa*)



Column	b_w	b_f	b_l	t	L	f_{crD}	f_{crL}	R_{DL}	f_{crG}/f_{crD}
WFSLC1	125	100	12	0.3055	1000	109.9	36.6	3.00	24.1
WFSLC2	125	100	12	0.3235	800	158.6	39.7	4.00	26.0
WFSLC3	140	100	12	0.3172	800	149.3	29.9	5.00	33.4
WFSLC4	140	80	12	0.3195	700	185.2	30.9	6.00	32.1
WFSLC5	140	80	12	0.26307	700	167.5	20.9	8.00	35.5
WFSLC6	140	80	12	0.22783	700	156.9	15.7	10.0	37.9

*in all columns, $d_1=d_3=10$ and $d_2=d_4=20$ mm.